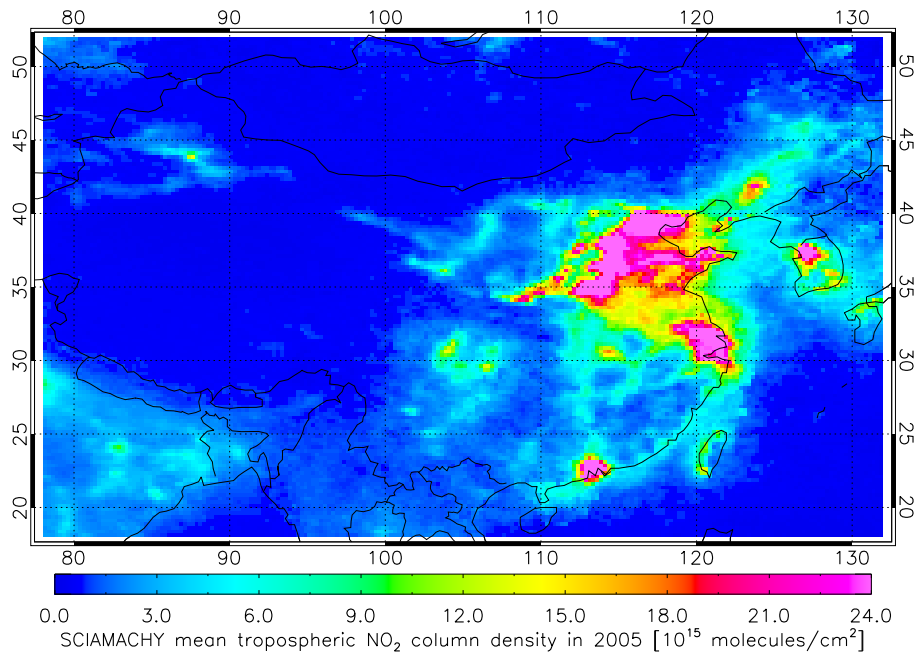


Anthropogenic NO_x emission estimates for China based on satellite measurements and chemistry-transport modelling



J.J.P. Kuenen

May 2006

Supervisors:

prof.dr. Hennie Kelder (KNMI, TUE)

dr. Ronald van der A (KNMI)

dr. Ernst Meijer (KNMI)

Abstract

Recent studies have shown that significant growth in tropospheric NO₂ has occurred over China, especially over its major cities. The main reason for this growth is the increase in anthropogenic NO_x emissions as a result from increasing power consumption and traffic. The purpose of this study is to improve the anthropogenic NO_x emission estimates in China, with the use of satellite observations from GOME and SCIAMACHY and the chemistry transport model TM5.

Firstly, the relationship between NO₂ columns and anthropogenic NO_x emissions is determined. Thereafter it is applied, in combination with satellite observations of tropospheric NO₂, to estimate the anthropogenic NO_x emissions in China. Multiple iterations have been performed to account for NO_x transport and to improve the emission estimates.

This approach has been applied to multiple years of data, whereafter a linear and exponential model have been used to fit the dataset. The results show that the exponential model fits better to the dataset and shows an increase of 20% in anthropogenic NO_x emissions in 2005.

Contents

1	Introduction	5
2	Atmospheric nitrogen oxides	9
2.1	Sources of NO_x	9
2.2	Relation with tropospheric ozone	10
2.3	NO_x sinks	13
3	Variability in NO_2	15
3.1	Seasonal cycle	15
3.2	Weekly cycle	17
3.3	Daily cycle	18
4	Satellite retrievals	21
5	The Chemistry Transport Model TM5	23
5.1	Description of the model	23
5.2	Emissions	24
5.3	Model set-up	26
6	Top-down estimate of anthropogenic NO_x emissions	29
6.1	Tropospheric NO_2 column response	29
6.2	Approximate linearity	31
6.3	A first top-down estimate	32
6.4	Iterative procedure	34
6.5	Discussion	35
7	Growing NO_x emissions in China	37
7.1	Emission estimates for other years	37
7.2	Annual emission trends	38
7.3	Global implications	40
8	Comparison to previous inventories	43
9	Seasonal variation in NO_2 columns	47
10	Conclusions and outlook	51

1

Introduction

Air pollution is a global problem with increasing importance. In Western countries, air pollution regulations have been taken and in general air quality has not deteriorated any further over the last decade. Regulations have been set for further improvement of air quality and reducing emissions of pollutants. In developing countries however, few measures against air pollution have been taken yet. Especially in countries with a fast-growing economy and no adequate regulations the air quality is deteriorating. An interesting example here is the P.R. China. The Chinese economy is growing rapidly with an averaged 9% per year. This has lead to an increase in emissions of pollutants, especially around the major cities.

One of the major pollutants in the troposphere are nitrogen oxides. The two most important nitrogen oxides in the troposphere are nitric oxide (NO) and nitrogen dioxide (NO₂). Because cycling between nitric oxide and nitrogen dioxide takes place on a time scale of a minute near the surface (during daytime), NO and NO₂ are often taken together and referred to as NO_x. Exposure to NO₂ can lead to health effects. They irritate the lungs and lead to lower resistance to respiratory infections such as influenza. Frequent exposure to concentrations that are typically much higher than those normally found in the ambient air may cause acute respiratory illness. Furthermore, NO₂ also leads to aerosol formation, which has also harmful health effects. Another serious problem of nitrogen oxides, in combination with hydrocarbons, is ozone production. Exposure to ozone may lead to a reduced lung function. During moderate exercise, even healthy people can suffer from chest pain, coughing, nausea and pulmonary congestion. Furthermore, tropospheric ozone is responsible for agricultural crop loss and damages forest ecosystems. (*Source: U.S. Environmental Protection Agency, 2006*)

Other environmental problems are caused by the removal of nitrogen oxides from the atmosphere. Most of the nitrogen oxides are removed from the atmosphere through the formation of HNO₃, which is one of the main components of acid rain. Also, an increase of nitrogen in surface waters leads to eutrophication.

Distributions of tropospheric NO₂ columns have been derived from the satellite instruments GOME aboard ERS-2, SCIAMACHY aboard Envisat and OMI aboard EOS-AURA [*Leue et al. (2001); Richter and Burrows (2002); Martin et al. (2002); Boersma et al. (2004); Bucselá et al. (2006)*]. Comparison of tropospheric NO₂ columns with in-situ and aircraft

measurements in the Po Valley and the Alps are described in *Petritoli et al.* (2004) and *Schaub et al.* (2006), respectively. A comparison between SCIAMACHY, the regional air quality model CHIMERE and in-situ measurements for western Europe has been made by *Blond et al.* (2005).

This study was carried out at KNMI between May 2005 and May 2006 in the framework of the "Air quality Monitoring and Forecasting In China" (AMFIC) project, which is a part of the DRAGON programme. Within this programme, European and Chinese scientists perform studies for the development of science and applications in the P.R. China. The programme is lead by the European Space Agency (ESA) and the Chinese Ministry of Science and Technology (MOST) and runs from 2004 to 2007. KNMI partners within the AMFIC project are the Belgian Institute for Space Aeronomy (BIRA-IASB), the Flemish Institute for Technological Research (VITO), the Netherlands organization for Applied Scientific Research (TNO-FEL), the University of Bremen, the National Satellite Meteorological Center of China (NSMC) and the Demokritus University of Thrace (DUTH). During this one-year study a work visit of one month to NSMC in Beijing has been made, where scientific data have been exchanged and study results have been presented.

An overview of the NO_x chemistry in the troposphere is given in chapter 2. Chapter 3 discusses the different cycles that can be distinguished in the variability of tropospheric NO_2 . Variations in anthropogenic activities and chemical activity in the atmosphere result in monthly, weekly and daily cycles in NO_2 . Measurements of NO_2 at ground level are used to determine the various cycles. The retrieval of tropospheric NO_2 columns from satellite is described in chapter 4 and chapter 5 describes the chemical transport model TM5. This model simulates concentrations of various trace gases in the troposphere, including NO_2 and tropospheric ozone.

This study is a continuation of the work of *Peters* (2005) and *van der A et al.* (2006a). Using satellite retrievals of tropospheric NO_2 from 1996 to 2004 from GOME [*Burrows et al.* (1999)] and SCIAMACHY [*Bovensmann et al.* (1999)], they found a significant growth in tropospheric NO_2 columns over China in the last decade, especially over major cities such as Shanghai and Beijing. The increase in NO_x emissions is the main reason for the steady growth in tropospheric NO_2 columns. However, it is difficult to quantify the increase in emissions based on the growth in tropospheric columns, because the non-linear NO_x chemistry and transport of NO_x between grid cells.

The goal of this study is to improve the anthropogenic NO_x emission estimates in China. To achieve this, first the response of the NO_2 tropospheric columns to a change in the NO_x emissions will be determined with the chemical-transport model TM5 [*Krol et al.* (2005)]. By matching the simulated tropospheric NO_2 columns to the tropospheric NO_2 columns from satellite observations for 2003, an optimized top-down emission inventory for this year is created. These procedures will be discussed in chapter 6. In chapter 7 this procedure will be repeated for the time period 1997-2005. The yearly NO_x emissions will be fitted to a linear as well as an exponential trend model. The NO_x emissions estimated in our top-down inventory will be compared to estimates from other studies in chapter 8.

By comparing monthly means, the differences in seasonal cycles between simulated and retrieved tropospheric NO_2 columns can be evaluated. The seasonal cycle in NO_2 observed by satellite has been studied by *van der A et al.* (2006a). The cycles shows a

winter maximum in East China, where anthropogenic emissions are dominant over natural emissions, while a summer maximum is found in West China. The comparison with the simulated seasonal cycle will be discussed in chapter 9. Finally, in chapter 10 we summarize the conclusions and make some recommendations for future work.

Part of the results of this study is used in the submitted paper by *van der A et al.* (2006b).

2

Atmospheric nitrogen oxides

In this chapter some aspects of tropospheric NO_x chemistry will be discussed. There are considerable differences between NO_x chemistry in the stratosphere and the troposphere. In the stratosphere, NO_x contributes to ozone destruction [*Jacob (1999)*], while in the troposphere the chemical regime determines whether ozone is produced or removed. In this chapter only the tropospheric chemistry will be discussed. NO_x in the troposphere influences ozone as well as hydroxyl (OH) concentrations. The latter is the primary oxidant in the troposphere and causes NO_x emissions to be oxidized, whereafter they are removed from the atmosphere by wet deposition. High ozone levels at the surface have serious health effects. In the upper troposphere high ozone levels also contribute to the greenhouse effect, since ozone is an efficient absorber of infrared radiation in the troposphere. In the stratosphere, roughly 90% of the total atmosphere's ozone is present, protecting the Earth from ultraviolet (UV) sunlight. The presence of NO_x and chlorine species (Cl and ClO) in the stratosphere leads to ozone destruction. This ozone destruction is well known from the Antarctic ozone hole. The influence of NO_x emissions on tropospheric ozone will be discussed in section 2.2.

2.1 Sources of NO_x

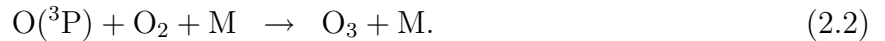
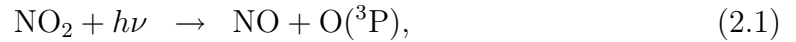
Most NO_x is emitted as NO from various anthropogenic and natural sources. NO is formed when N_2 and O_2 molecules break at high temperatures ($T > 1000$ K). The main anthropogenic source is fossil fuel combustion, mainly caused by traffic and heavy industry. Major natural sources include lightning and soil emissions. *Olivier et al. (1998)* estimate that 75% of the yearly global NO_x emissions are coming from anthropogenic sources and roughly 50% of the total NO_x sources is accounted for by fossil fuel combustion only. The largest natural sources are soil emissions, oxidation of NH_3 emitted by the biosphere and NO_x emissions from lightning. The latter accounts for roughly 10% of the total NO_x emissions [*Boersma et al. (2005)*]. Table 2.1 gives an overview of the main tropospheric sources of NO_x .

Source	<i>Jacob</i> (1999)	EDGAR 3.2
Fossil fuel combustion & industry	21	26.6
Biomass burning & biofuel	12	6.5
Aircraft emissions	0.5	0.6
Total anthropogenic sources	33.5	34.4
Soils	6	
NH ₃ oxidation*	3	
Lightning	3	
Transport from stratosphere	0.1	
Total natural sources	12.1	
Grand total	46.6	

Table 2.1: Global tropospheric sources of NO_x emissions in Tg N per year, data from *Jacob* (1999) and the EDGAR 3.2 database [*Olivier and Berdowski* (2001)] for anthropogenic NO_x emissions. *Is also partly an anthropogenic source, since it contains substantial contributions of agriculture.

2.2 Relation with tropospheric ozone

Ozone in the troposphere is mainly produced by photolysis of NO₂ and consists of

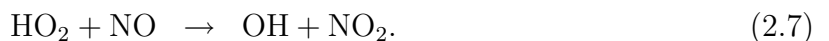
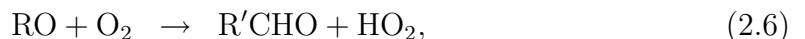
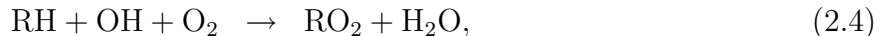


The reaction of ozone with NO regenerates NO₂:



Reactions (2.1)-(2.3) constitute a cycling between NO and NO₂ with no net production of O₃. During nighttime, most NO_x is present as NO₂, because there is no light to photodissociate NO₂ into NO via (2.1).

Without any further reactions, the cycling reactions (2.1)-(2.2) and (2.3) are in equilibrium. However, in the presence of CO, CH₄ or non-methane hydrocarbons (NHMC), NO can be converted to NO₂ without destroying ozone. This conversion process occurs in the presence of abundant OH. For NHMC and CH₄ it consists of the following set of reactions:



In this set of reactions, (2.5) and (2.7) provide the alternative pathways for (2.3) to form NO₂ that can be photolyzed and produce O₃. In (2.6), R' represents an organic fragment

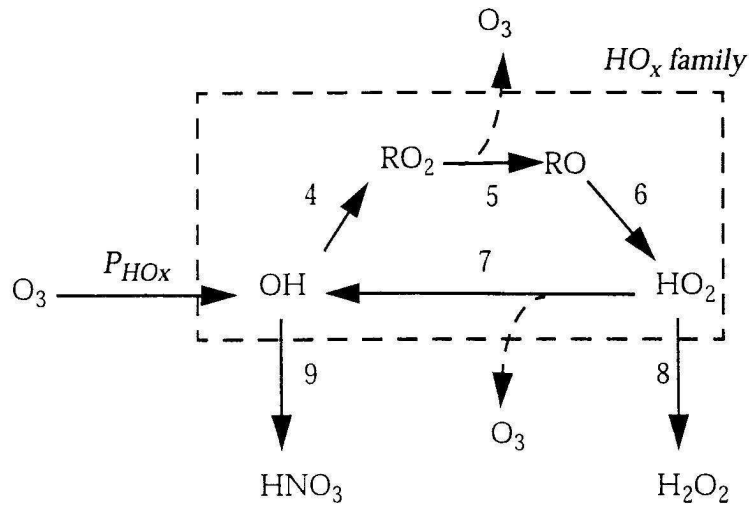
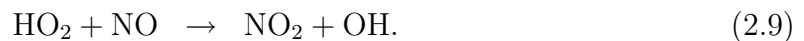
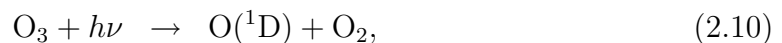


Figure 2.1: Chain reaction resulting in a net ozone production. Picture taken from *Jacob (1999)*.

with one carbon atom less than R. In the presence of CO, the conversion process is slightly different:

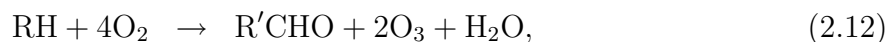


The set of reactions (2.4)-(2.7) and (2.8)-(2.9) lead to an increase in OH, because tropospheric ozone is the major source of OH. In this way ozone is removed from the atmosphere:



Other possible removal reactions for O₃ are reactions with OH or HO₂ in the remote troposphere, or reaction with organic materials at the surface of the Earth (dry deposition).

The net reaction for the earlier described mechanisms for ozone production (2.4)-(2.7) and (2.8)-(2.9), respectively, is given by



In (2.12), R'CHO will be oxidized further leading to additional NO₂ formation. Ultimately, all hydrocarbons will form CO₂. This chain reaction is displayed in figure 2.1 and will terminate when no more HO_x is available. The figure shows two possible ways for this to happen.

The high NO_x case

For very high NO_x emissions, typical for present-day continental boundary layers, the most important process to end the chain reaction is oxidation of NO_2 according to



The ozone production rate of the chain process described by (2.4)-(2.7) can be written as

$$P_{\text{O}_3} = k_5[\text{RO}_2][\text{NO}] + k_7[\text{HO}_2][\text{NO}]. \quad (2.15)$$

Here, the reactions coefficient number k_i refer to reaction i displayed in figure 2.1. Assuming efficient chain propagation, meaning equal reaction rates k_4 - k_7 , leads to

$$P_{\text{O}_3} = 2k_7[\text{HO}_2][\text{NO}]. \quad (2.16)$$

Efficient cycling implies a steady state for OH considering production from (2.7) and removal from (2.4). This yields

$$[\text{OH}] = \frac{k_7[\text{HO}_2][\text{NO}]}{k_4[\text{RH}]}. \quad (2.17)$$

Furthermore, production of HO_x is constant and can be written as:

$$P_{\text{HO}_x} = k_8[\text{HO}_2]^2 + k_9[\text{NO}_2][\text{OH}][\text{M}]. \quad (2.18)$$

For very high NO_x emissions, the dominant sink for HO_x is oxidation of NO_2 . Therefore, the first term on the right hand side of (2.18) can be neglected. This equation can be combined with (2.17):

$$P_{\text{HO}_x} = \frac{k_7k_9[\text{NO}][\text{NO}_2][\text{HO}_2][\text{M}]}{k_4[\text{RH}]}. \quad (2.19)$$

Substituting (2.19) into (2.16) then yields for the ozone production rate:

$$P_{\text{O}_3} = \frac{2k_4P_{\text{HO}_x}[\text{RH}]}{k_9[\text{NO}_2][\text{M}]}. \quad (2.20)$$

The ozone production rate varies linearly with the hydrocarbon concentration, and inversely with the NO_2 concentration. As long as the concentration of hydrocarbons is sufficiently low, reducing NO_x emissions leads to an *increase* in ozone production. This is illustrated in figure 2.2. Because the ozone production rate is limited by the hydrocarbons, this regime is called the *hydrocarbon-limited regime*.

The low NO_x case

For relatively low NO_x concentrations, the dominant reaction in ending the chain reaction is



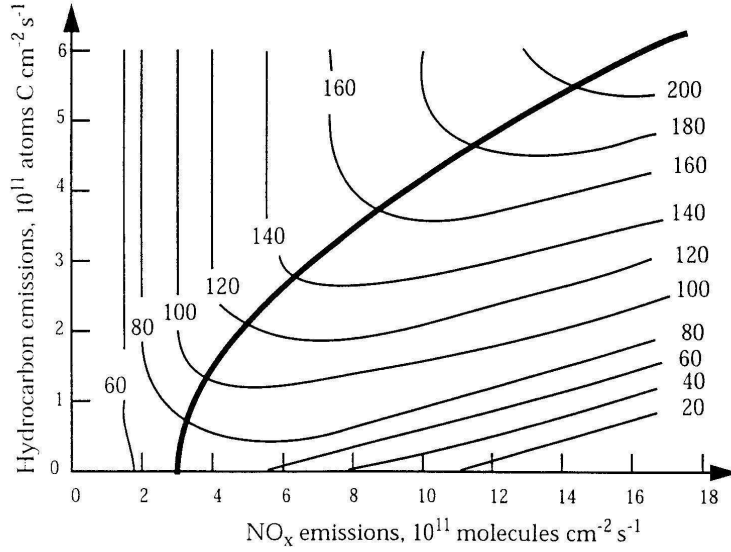


Figure 2.2: Ozone concentrations [ppbv] simulated by a regional photochemical model, as a function of NO_x and hydrocarbon emissions. The thick line separates the NO_x -limited regime (top left) and the hydrocarbon-limited regime (bottom right). The figure is taken from *Sillman et al.* (1990).

Therefore the second term on the right hand side of (2.18) can be neglected. Substituting (2.18) into (2.16) then yields for the ozone production rate:

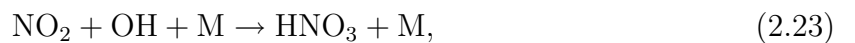
$$P_{\text{O}_3} = 2k_7 \sqrt{\frac{P_{\text{HO}_x}}{k_8}} [\text{NO}]. \quad (2.22)$$

For low NO_x concentrations the O_3 production varies linearly with the NO concentration and is independent of the hydrocarbon concentrations. Because the ozone production rate is limited by the NO_x concentration, this case is referred to as the *NO_x -limited regime*. The ozone production in this regime is more efficient than in the hydrocarbon-limited regime, because in the NO_x -limited regime, OH will also react with NO_2 and therefore be removed from the reaction cycle.

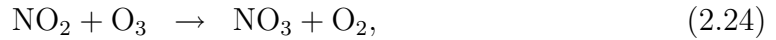
The two regimes (for high and low NO_x concentrations) are schematically shown in figure 2.2. The thick line separates the NO_x -limited regime and the hydrocarbon-limited regime.

2.3 NO_x sinks

The main sink for NO_x starts with the oxidation of NO_2 , during daytime via:



and at night, when no OH is present, via



where the latter reaction requires the presence of aerosols. In these reactions, M represents a molecule (usually N_2 or O_2) that absorbs the energy that is released in this reaction. Because HNO_3 is highly soluble in water, it is likely to be scavenged by rain whereby NO_x is removed from the atmosphere. Because of this quick removal, the lifetime of NO_x in the atmosphere is short. It varies from a few hours in the boundary layer up to several days in the upper troposphere. Therefore NO_x is unlikely to be transported far from its source. However, if NO_x is transported higher into the troposphere by convection, there is an efficient mechanism for long-range NO_x transport: peroxyacetylnitrate ($\text{CH}_3\text{C}(\text{O})\text{OONO}_2$) or PAN, for short, is produced from photochemical oxidation of carbonyl compounds in the presence of NO_x . The lifetime of PAN is strongly temperature-dependent and can be up to several months when T is sufficiently low ($T \sim 250$ K). Because PAN is much less soluble in water it can be transported by large distances, before it decomposes and NO_x regenerates. Generally, this NO_x is lost again via (2.23). However, there are also converse reactionpaths from HNO_3 to NO_x . Since the OH production rate depends non-linear on the NO_x concentration [*Logan et al.* (1981)], the amount of NO_x that is lost due to HNO_3 formation depends on the NO_x concentration as well.

3

Variability in NO₂

Concentrations of NO₂ in the atmosphere depend on production, removal, transport and the chemical reactions. In the NO₂ concentrations in the atmosphere, distinct cycles can be distinguished between summer and winter, between weekdays and weekends, and between day and night. To get better insight in these cycles, they will be visualized in this chapter using in situ NO₂ measurements from stations around Hong Kong and from stations in Europe. Differences between Chinese and European stations will be discussed in detail.

3.1 Seasonal cycle

In East China, where anthropogenic emissions are dominating, the NO₂ tropospheric columns are typically higher in the winter [*van der A et al. (2006a)*]. The changing amount of sunlight is the principle driver of this variability. Sunlight triggers OH production, causing NO₂ to be removed from the atmosphere by (2.23). Since sunlight is reduced in winter, there will be less NO₂ removal in that season, causing NO₂ concentrations to increase. Also heating during winter with enhanced NO_x emissions as a result, plays a role. In West China however, a summer maximum in NO₂ is found, which is attributed to higher lightning and soil NO_x emissions in summer. In *Van der A et al. (2006a)* the typical difference between summer and winter NO₂ tropospheric columns is estimated to be in the order of $1.0 \cdot 10^{15}$ molecules cm⁻².

The tropospheric column contains NO₂ in the boundary layer as well as in the free troposphere. In the boundary layer, the NO₂ concentrations near the Earth's surface are much more affected by changes in emissions than the NO₂ concentrations higher in the troposphere. Therefore, the amplitude of the seasonal cycle is expected to be higher for in situ measurements than for the tropospheric column.

Hourly NO₂ measurements from various stations in and around Hong Kong have been collected. These data are provided by the Environmental Protection Department of the Government of Hong Kong [*EPD (2005)*]. The Central/Western station is located at the western part of Hong Kong island near the ocean, and Kwun Tong is located just off Hong Kong island in Kowloon. Figure 3.1 shows the seasonal behavior of ground-level NO₂ at both these stations. For comparison, the same figure also contains a similar plot for 2 stations in Europe. The European data are supplied by the World Data Centre for

Greenhouse Gases (WDCGG). Station Kollumerwaard is a background station located in the northern part of the Netherlands, where anthropogenic activity is less than in the middle and southern part of the country. The station Stephansplatz is located in the city center of Vienna, Austria. The exact location and altitude of all stations is given in table 3.1.

Station	Latitude	Longitude	Altitude
Kollumerwaard (Netherlands)	53°20'	6°17'	0 m
Stephansplatz (Austria)	48°13'	16°23'	171 m
Central/Western (China)	22°16'	114°08'	18 m
Kwun Tong (China)	22°18'	114°13'	25 m

Table 3.1: Longitude, latitude and altitude of the ground stations in Europe and China.

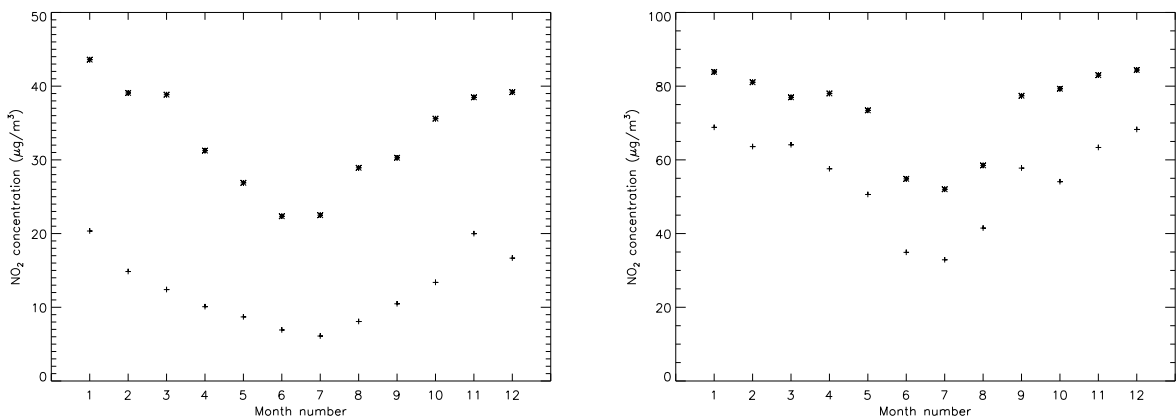


Figure 3.1: Left panel: Averaged NO₂ concentrations for every month (1=January, 12=December) for stations Kollumerwaard (Netherlands) [+] and Stephansplatz (Austria) [*]. Right panel: Average NO₂ concentrations for every month for stations Central/Western [+] and Kwun Tong [*], both in the Hong Kong area. Data are averaged for every month in 1997-2001. Note that the vertical scales are different.

From the figure it can be seen that, both in Europe and China, winter NO₂ concentrations exceed the summer NO₂ concentrations roughly by a factor of 2 in the boundary layer. For China, the difference between summer and winter is slightly smaller than for Europe. Since the Chinese stations are located closer to the equator, the difference in the amount of sunlight between summer and winter is less than at the European stations. Lower NO₂ concentrations at the two Hong Kong stations are mainly found during the three months June, July and August. This might be explained by the fact that these three months form the rainy season in Hong Kong. During rain, NO_x is more efficiently removed from the atmosphere via HNO₃.

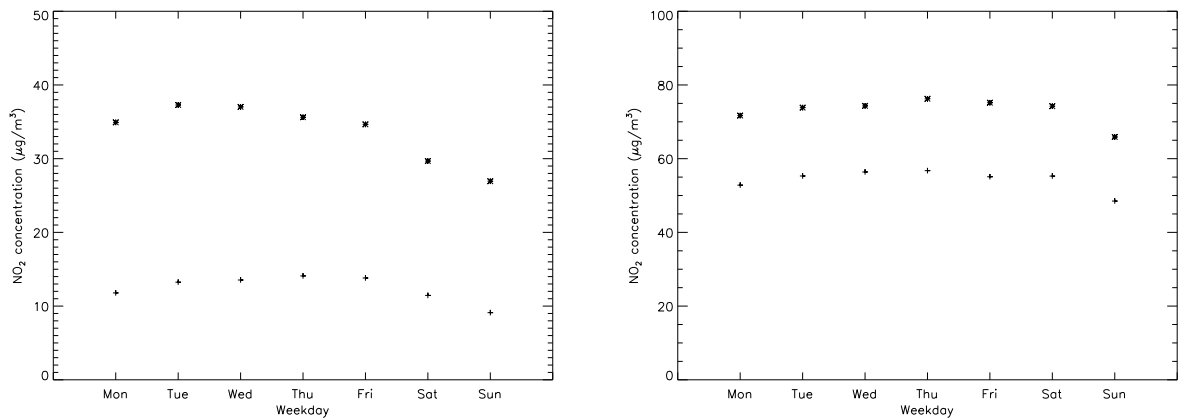


Figure 3.2: Left panel: averaged NO_2 concentrations for every day of the week for stations Kollumerwaard (Netherlands) [$+$] and Stephansplatz (Austria) [$*$]. Right panel: averaged NO_2 concentrations for every day of the week for stations Central/Western [$+$] and Kwun Tong [$*$], both in the Hong Kong area. Data are averaged for 1997-2001.

3.2 Weekly cycle

Anthropogenic activity is reduced in weekends with respect to weekdays, especially in western countries with a Christian tradition, which is expected to be visualized by a decrease in NO_2 tropospheric columns during the weekend. *Beirle et al. (2003)* found these weekly cycles in NO_2 tropospheric columns in GOME retrievals. In Europe and the US, they observed the expected decrease in NO_2 on Sundays. In China however, they found no indication for a weekly cycle. They assumed that NO_x emissions in East China are dominated by heavy industry and power plants that also run in the weekend.

Figure 3.2 shows the NO_2 weekly cycle for the two stations in Hong Kong and the two stations in Europe. First, daily averages are determined from the hourly NO_2 data. From these daily averages a weekly cycle is constructed. For the European stations, the figure shows a decrease in NO_2 concentration on Saturday and an even lower value on Sunday. Furthermore, the NO_2 values are higher in the middle of the week, while slightly lower average NO_2 concentrations are measured on Monday and Friday. In Hong Kong however, the average NO_2 concentrations are more or less equal for every weekday, except for Sunday when the average NO_2 concentration is about 10% lower. Since most people do have free weekends in China, this decrease is expected. However, *Beirle et al. (2003)* did not find a decrease in NO_2 on Sunday in China. Perhaps Hong Kong is not very representative for China in the sense that it is much more oriented to the Western world than the rest of China. Another possible explanation is that the 10% difference is within the error in the retrieval from GOME.

The decrease on Sundays in Hong Kong is lower than the decrease that is measured in Europe, which is about 20-30%. This indicates that power generation and heavy industry, that run throughout the week, are important NO_x emitters in Hong Kong.

However, while the ground station data show a minimum NO_2 concentration on Sundays, the minimum GOME NO_2 columns found by *Beirle et al. (2003)* over Hong Kong

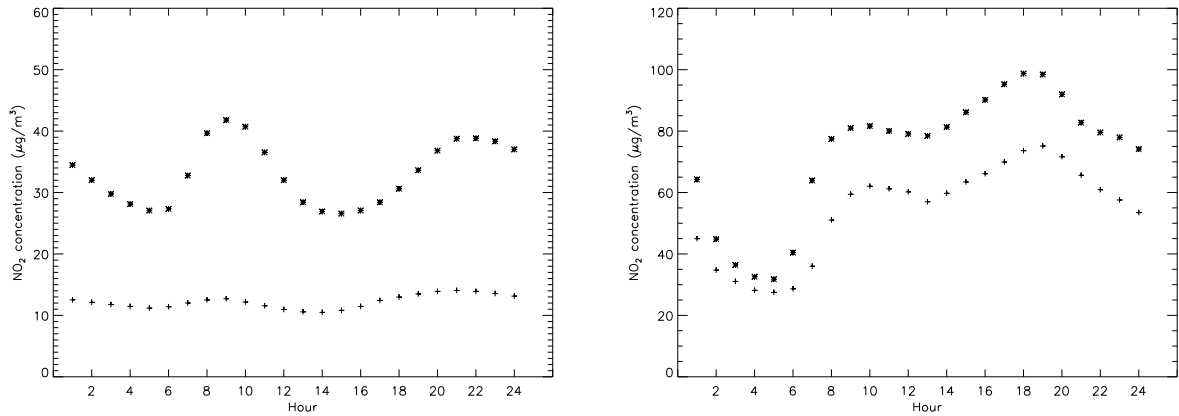


Figure 3.3: Left panel: yearly averaged hourly NO₂ concentrations for stations Kollumerwaard (Netherlands) [+] and Stephansplatz (Austria) [*]. Right panel: yearly averaged hourly NO₂ concentrations for stations Central/Western [+] and Kwun Tong [*], both in the Hong Kong area. Data are averaged for 1997-2001.

are on Tuesday, Wednesday and Thursday, rather than in the weekend. It is not straightforward to compare in situ measurements to columns, but a minimum on weekdays is not expected. Since the decrease is small, it might be accounted for by errors in the GOME retrieval or due to its large ground pixel as compared to the extend of the Pearl River Delta region.

3.3 Daily cycle

As mentioned in chapter 2, NO_x chemistry is very different for day and night. At night, there is no sunlight to produce the radicals and no ozone or HO_x will be formed. Also NO_x emissions will generally be lower in the night. Since a significant part of the NO_x emissions comes from traffic, higher NO_x concentrations are expected during rush hours. *Lelieveld and Helas* (1987) show that in the early morning first the NO concentration is rising due to increased anthropogenic activity. When the sun rises, NO is removed and NO₂ produced consuming ozone. Later in the morning, less NO is present due to less traffic, whereafter also NO₂ concentrations are going down. The same pattern can be seen during the evening rush hour. Due to the fact that it is mainly NO that is emitted and then transformed to NO₂ in the presence of ozone, the NO₂ peak is found just after the rush hour.

Figure 3.3 shows hourly NO₂ variations for the two European and the two Chinese stations. Data are averaged over the 5-year period 1997-2001. For the European station, two peaks are found as expected. The first represents the morning rush hour and the second the evening rush hour. The amplitude of the daily variations is larger for Stephansplatz compared to Kollumerwaard. This is due to the location of Stephansplatz, in the center of Vienna, while Kollumerwaard is located in a much less populated area.

The two Hong Kong stations show a different daily cycle. The two datasets in figure 3.3 show NO₂ concentrations with very large variations during the day. In morning rush

hour the NO_2 concentration is growing rapidly to a local maximum. Then there is a small decrease until approximately 1 p.m. From that moment, a steady increase is visible towards its highest value around 7 p.m. After this time a steady decrease towards the minimum value around 5 a.m. in the morning can be seen. The maximum NO_2 concentration can be 3 times as high as the minimum. Apparently, there is a large difference between the amount of NO_x emissions during day and night in Hong Kong. A possible explanation for the constantly high NO_2 concentration during daytime is ozone titration. This leads to a decrease in the OH concentration, limiting the removal of NO_2 from the atmosphere via HNO_3 . At night however, NO_2 is removed from the atmosphere without consuming OH via (2.24)-(2.26). This might explain the strong decrease in NO_2 during nighttime. It can also be seen that NO_2 concentrations in Hong Kong start to decrease around 6 or 7 p.m., while in Europe this will not start before approximately 10 p.m. Because of the lower latitude in Hong Kong, in summer the sunset is earlier than in Europe and as a consequence NO_2 concentrations start to decrease earlier as well.

4

Satellite retrievals

Observations of tropospheric NO_2 are provided by the satellite instruments GOME and SCIAMACHY. These instruments are spectrometers, measuring backscattered light from the Earth's surface and atmosphere. Incoming sunlight is scattered back from molecules in the atmosphere. Because the absorption of the molecules depends on the wavelength, backscattered light from different molecules can be distinguished. The spectral range of backscattering from NO_2 molecules is 425–450 nm. The amount of absorption is calculated by comparing the spectrum to a reference spectrum and can be used to calculate the atmospheric concentration of the specific molecule.

Both GOME and SCIAMACHY fly a sun-synchronous orbit, which means they are crossing the equator at the same local time every orbit. These overpass times at the dayside of the Earth are 10.30am for GOME and 10.00am for SCIAMACHY. The Global Ozone Monitoring Instrument (GOME) was launched aboard ERS-2 in April 1995. NO_2 data from GOME are available from early 1996. The satellite looks straight down (nadir view) observing the atmosphere with a pixel size of 320 km by 40 km. GOME provides global coverage every 3 days and measures atmospheric concentrations of O_3 , NO_2 , SO_2 , BrO, H_2CO , H_2O and aerosols. SCIAMACHY (SCanning Imaging Absorption spectroMeter for Atmospheric CartographY) is on board ESA's ENVISAT platform. Its pixel size is 60 km by 30 km. NO_2 tropospheric columns from SCIAMACHY are available from January 2003. SCIAMACHY has the ability to look forward through the atmosphere (limb view), as well as to monitor in nadir view. Because SCIAMACHY is alternating between nadir and limb measurements and for tropospheric NO_2 observations only nadir observations are used, global coverage is achieved every 6 days. Besides NO_2 , SCIAMACHY also detects O_3 , SO_2 , BrO, H_2CO , H_2O , CO, CO_2 , CH_4 , N_2O and aerosols. The pixel sizes of GOME and SCIAMACHY are schematically shown in figure 4.1.

Three steps are necessary to convert the observed spectra to tropospheric NO_2 columns. First, the observed spectrum is converted into a slant column density by BIRA-IASB using the Differential Optical Absorption Spectroscopy technique [Platt (1994)]. This technique fits the spectrum with a model describing absorption and scattering on clouds, aerosols and air molecules. Secondly, the total column data is assimilated using the chemistry-transport model TM4 [Dentener *et al.* (2003)], which is an off-line model driven by meteorological fields from ECMWF. Subtracting the assimilated stratospheric slant column from the to-

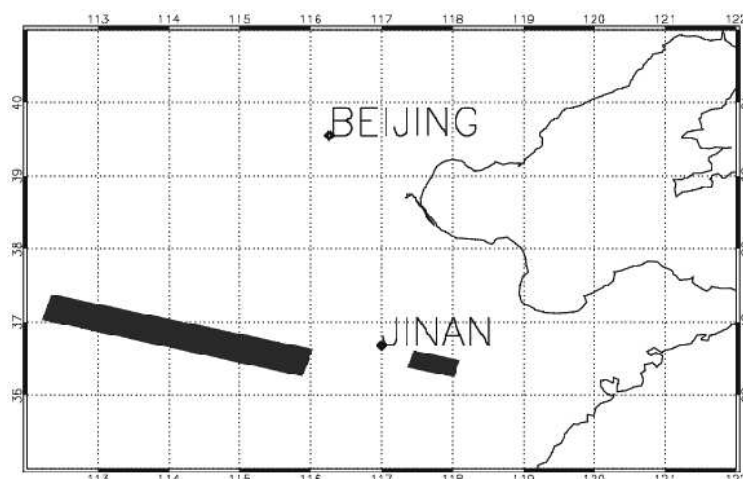


Figure 4.1: Example of the pixel size of GOME (large pixel) and SCIAMACHY (small pixel) over China.

tal slant column yields the tropospheric slant column. Finally, the vertical tropospheric NO_2 columns are derived, based on calculations with the Doubling-Adding KNMI (DAK) model in combination with the modelled tropospheric NO_2 profiles from the TM4 model. Retrievals are only used when the radiance reflectance is less than 50%, corresponding to a cloud fraction of less than about 20%. The cloud fraction and cloud top-height are calculated from the observations using the well-validated FRESCO algorithm [Koelemeijer *et al.* (2003)]. To account for this cloud filtering, we use yearly averaged tropospheric NO_2 columns that are determined by averaging monthly mean tropospheric NO_2 columns.

Tropospheric NO_2 columns from GOME, SCIAMACHY are publicly available on the TEMIS project website (www.temis.nl), including error estimates and kernel information [Eskes and Boersma (2003)]. In the future, also NO_2 columns from the Ozone Monitoring Instrument (OMI), launched in 2004 aboard EOS-AURA, will become available.

5

The Chemistry Transport Model TM5

5.1 Description of the model

In this study, the chemistry transport model TM5 [Krol *et al.* (2005)] is used for the modelling of atmospheric NO₂ concentrations. This model has been developed jointly by the Royal Netherlands Meteorological Institute (KNMI), the Institute for Marine and Atmospheric Physics at Utrecht University (IMAU) and the Institute for Environment and Sustainability of the EU Joint Research Center (EI-JRC) in Ispra, Italy. The highest resolution of the model is 1×1° (longitude × latitude). One of the advanced features of this model is its zoom capability. Model simulations can be performed on a coarse scale globally, while a selected region can be examined in much more detail. The central idea behind this zooming technique is that the global coarse resolution represents the main transport features and serves as a boundary condition for the regional zoom domain. In a zoom region, the model runs simultaneously at various resolutions. There can be more than one zoom region, every region can have a coarser region (parent) and a finer resolved region (child). The zooming algorithm is two-way: the parent provides the boundary conditions for its children and the children update the information of the parent. There is also a refinement in time for the children, if region 1 is solved with a timestep ΔT , then region 2 is solved with timestep $\Delta T/2$ and region 3 with $\Delta T/4$.

The model basis is the continuity equation, which for every tracer can be written as

$$\frac{\partial \rho}{\partial t} + \nabla \cdot (\rho \vec{v}) = \tilde{Q}, \quad (5.1)$$

where ρ represents the mass or number density and \tilde{Q} the chemical source term [Brasseur *et al.* (1999)]. Furthermore, \vec{v} represents the transport velocity vector and t is time. The chemical term \tilde{Q} depends explicitly on time and spatial components, but also on the densities. In chemistry transport models, this equation is rewritten in terms of the mixing ratio vector $\mu = \rho/\rho_a$ and $S = \tilde{Q}/\rho_a$, where ρ_a represents the total atmospheric mass or

number density. This yields

$$\frac{d\boldsymbol{\mu}}{dt} = \frac{\partial\boldsymbol{\mu}}{\partial t} + \vec{v} \cdot \vec{\nabla}\boldsymbol{\mu} = \mathbf{S}. \quad (5.2)$$

Together with initial and boundary conditions, the latter equation forms the heart of the model. Unfortunately it is not possible to solve this equation analytically in most cases. The differential equations are replaced by discrete analogues, whose solutions are calculated for every grid cell and every time step individually. Within every grid cell, the transport, emissions, deposition and chemistry of tracers is solved by means of operator splitting. This means for every time step these processes are solved separately [Berkvens *et al.* (1999)]. A basic requirement for the model is positiveness of the tracer concentrations. Large-scale advection is modelled using the slopes scheme of Russell and Lerner (1981). TM5 uses different parametrization schemes for physical processes that cannot be explicitly resolved due to the coarseness of the grid. The parameterisation of convection is based on Tiedtke (1989) and diffusion is calculated using a diffusion scheme based on Holtslag and Boville (1993).

The model uses a Carbon Bond Mechanism 4 (CBM-4) scheme modified for tropospheric chemistry [Houweling *et al.* (1998)], containing full HO_x-NO_x-SO_x-CO-CH₄-NHMC chemistry. In this scheme 38 gaseous constituents are considered, of which 23 tracers are transported. A total of 110 gas phase reactions and 24 photolysis reactions are taken into account. Dry deposition is based on a parameterisation of Ganzeveld *et al.* (1998) and wet deposition is accounted for by a parameterisation of Junge and Gustafson (1957) and Langner and Rodhe (1991). Heterogeneous removal of N₂O₅ on sulphate aerosols is described using a parameterisation by Dentener and Crutzen (1993). Since this chemical scheme does not include sufficient stratospheric chemistry, a zonally and monthly mean O₃ climatology [Fortuin and Kelder (1998)] scaled with TOMS total O₃ measurements is prescribed above 50 hPa. Transport of HNO₃ from the stratosphere into the upper level of the model is accounted for by fixing the O₃/HNO₃ ratio in the model top layer, based on UARS derived O₃/HNO₃ ratios at 10 hPa.

TM5 works with 60 hybrid sigma-pressure levels, identical to the forecast model used by the European Center for Medium Range Weather Forecast (ECMWF). The tropospheric standard version used in this study uses 25 vertical layers, where the first 5 levels describe the boundary layer, the next 10 the free troposphere and the last 10 the stratosphere.

TM5 is an off-line model, which means that it depends on meteorological data calculated by a climate model or weather forecast. These meteorological data are provided by the IFS-model of ECMWF [ECMWF (2002)]. The meteorological data have to be pre-processed before running the model and stored on disks or tape.

5.2 Emissions

TM5 uses information from different emission databases for its input emissions. Most of the NO_x emissions based on estimates of version 3.2 of the Emission Database for Global Atmospheric Research (EDGAR 3.2) [Olivier and Berdowski (2001)], which has been released in 2001. EDGAR is a joint project of the National Institute for Public

Health of the Netherlands (RIVM) and the Netherlands Organization for Applied Scientific Research (TNO). The database is linked into and part of the Global Emissions Inventory Activity (GEIA). Version 3.2 is based on the year 1995, scaled to 1997 and contains the latest information available at that time.

EDGAR 3.2 emissions are provided in different categories for every pollutant, describing the main source of the emission. The following major categories are defined in the EDGAR 3.2 emission database:

- F : Fossil fuel use
- I : Industrial processes
- B : Biofuel combustion
- L : Agriculture and biomass burning (land use)
- W : Waste handling

These main categories are split up in subcategories, describing the detailed emission source. For instance, for fossil fuel emissions the following different subcategories are defined:

- F10 : Industry (excluding coke ovens, refineries, etc.)
- F20 : Power generation (public and auto; including cogeneration)
- F30 : Other transformation sector (refineries, coke ovens, gas works, etc.)
- F40 : Residentials, Commercial and Other Sector (RCO)
- F51 : Road transport
- F54 : Non-road land transport (e.g. rail, inland water)
- F57 : Air transport
- F58 : Shipping transport
- F70 : Coal production
- F80 : Oil production, transmission and handling
- F90 : Gas production and transmission

As can be seen from the list, the F50 category contains the emissions from transport and is split up in four different transport sources. The complete list of emission categories can be found at the Edgar website www.rivm.nl/edgar. Anthropogenic emissions are defined as the sum of all the emissions from the F and I main categories. All other emissions, including NO_x emissions from lightning, are referred to as natural NO_x emissions.

Fossil fuel, industrial and biomass NO_x emissions are taken from this database, except for the air transport category (F57). NO_x aircraft emissions are taken from the ANCAT/EC2 database [*Gardner (1998)*]. Lightning NO_x emissions are calculated in the model, depending on meteorological parameters [*Meijer et al. (2001)*]. The global annual NO_x emission from lightning is approximately 5 Tg N. Soil NO_x emissions are given as monthly means based on the parameterisation of *Yienger and Levy (1995)*.

Apart from the NO_x emissions, anthropogenic emissions of CO, CH₄ and NMHC are also taken from the EDGAR 3.2 database. Anthropogenic SO₂ emissions are from IIASA & GEIA.

This emission database has been constructed by combining various available statistic datasets. However, for China little data were available to construct this dataset, and trends

in East-China tropospheric NO_2 indicate that the NO_x emissions are rapidly increasing. Therefore, this study aims to quantify the NO_x emissions in China on the basis of satellite observations of NO_2 . The total of global NO_x emissions used in the model per category is shown in table 5.1. Emissions for China are also shown in this table.

Category	Global	China
Fossil fuel combustion & industry	26.6	3.32
Biofuel	2.4	0.44
Biomass burning	4.2	0.01
Aircraft emissions	0.9	0.02
Soil emissions	4.1	0.03
Total	38.2	3.82

Table 5.1: Totals of NO_x emissions in TM5, both at a global scale and for China. Emission units are Tg N per year. Calculated totals do not contain NO_x emissions from lightning and oxidation of NH_3 .

5.3 Model set-up

For the runs that were performed for this study, a global resolution of $6\times 4^\circ$ was used while a smaller rectangular area, in which China is included, is resolved at a $1\times 1^\circ$ resolution. A larger rectangular Chinese domain was resolved on a $3\times 2^\circ$ resolution in this setup to allow a smooth transition from the $6\times 4^\circ$ to the $1\times 1^\circ$ region. Table 5.2 states the different regions and figure 5.1 depicts them on a world map.

Region number	Resolution	Longitudes	Latitudes
1	$6\times 4^\circ$	-180 - 180	-90 - 90
2	$3\times 2^\circ$	66 - 144	10 - 58
3	$1\times 1^\circ$	78 - 132	18 - 52

Table 5.2: Definition of the zoom regions used in this study.

NO_2 concentrations vary significantly during the day, as pointed out in section 3.3. The satellite instruments GOME and SCIAMACHY both fly a sun-synchronous polar orbit, thus always crossing the equator at the same local time: 10.30am and 10.00am for GOME and SCIAMACHY, respectively. To make a correct comparison between the model and the satellite retrievals, the model output should be given at the same time. A new subroutine within TM5 generates output at this local time every day, and produces a monthly average of these daily concentrations at the end of the month. In the output files not only the 3D mixing ratios are given, but also 2D tropospheric columns are calculated within the subroutine. The tropospheric NO_2 column is obtained by vertically integrating the NO_2

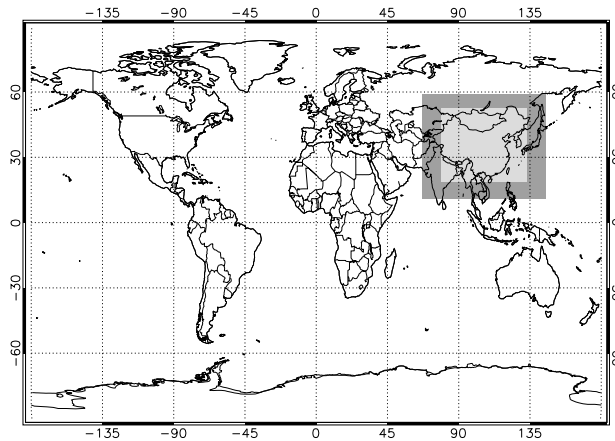


Figure 5.1: The 3 regions in the model. The whole world is simulated at a resolution of $6 \times 4^\circ$ (longitude x latitude). The light grey area is resolved at a resolution of $1 \times 1^\circ$ (longitude x latitude). To allow a smooth transition between the two regions, the rectangular area represented by the dark & light grey areas is resolved at $3 \times 2^\circ$.

mixing ratios from the Earth surface until the top of the troposphere, which is taken at 200 hPa.

6

Top-down estimate of anthropogenic NO_x emissions

Trend studies [*van der A et al. (2006a)*; *Richter et al. (2005)*] based on satellite retrievals have shown a significant growth in tropospheric NO_2 columns in China over the last decade, which they attributed to the growth in anthropogenic NO_x emissions. However, quantifying the relation between the local observed NO_2 tropospheric column and the actual NO_x emission is complicated because of the non-linear NO_x chemistry and transport of NO_x between grid cells.

In this chapter a procedure to estimate the anthropogenic NO_x emissions for 2003 in China will be presented, based on the observed tropospheric NO_2 columns for that year. The inversion procedure here described is an adapted version of the one of *Martin et al. (2003)*. In this chapter, we will only estimate the anthropogenic NO_x emissions from fossil fuel combustion and industry. All other emissions will be referred to as natural emissions and will not be estimated in this chapter.

To obtain the anthropogenic NO_x emissions from the tropospheric NO_2 column, the relation between column and emission is determined for every grid cell by simulating the tropospheric NO_2 columns for a wide range of anthropogenic NO_x emissions. This relation will be applied to satellite observations of tropospheric NO_2 , thus obtaining an estimate for the anthropogenic NO_x emission.

6.1 Tropospheric NO_2 column response

In order to determine the response of the tropospheric NO_2 column to the input emissions, a series of TM5 simulations have been performed, whereby the anthropogenic emissions (EDGAR 3.2) have been scaled with a constant emission multiplication factor (EMF). These factors were 0.5, 1, 1.5, 2, 4, 6 and 8. Yearly averaged tropospheric NO_2 columns for 2001 have been calculated from the modelled monthly mean tropospheric columns. When comparing two yearly averaged columns, the local response R of the tropospheric NO_2

column Ω_i to a change in the anthropogenic emission $E_{ant,i}$ is defined as

$$R = \frac{\frac{\Omega_2}{\Omega_1} - 1}{\frac{E_{ant,2}}{E_{ant,1}} - 1}. \quad (6.1)$$

The response R varies between 0 and 1. A zero response (indicating that the tropospheric NO₂ column does not change when anthropogenic emissions are increased) indicates that no anthropogenic emissions are present in that particular grid cell. On the other hand, a response of 1 is an upper limit when e.g. a factor 2 increase in the anthropogenic emission leads to a factor 2 increase in tropospheric NO₂ column. The response factors will be affected by transport of NO_x between grid cells, especially in regions with high gradients in tropospheric NO₂. The left panel of figure 6.1 is an example of such a response map, where the simulations with EMF=2 and EMF=1 are compared. The figure shows a high response ($R > 0.5$) for areas with high anthropogenic emission levels. This is explained by the fact that only anthropogenic NO_x emissions are increased. At locations with only natural emissions the response will always be zero, if transport effects would be neglected. The ratio of anthropogenic and natural NO_x emissions determines the maximum response of a grid cell.

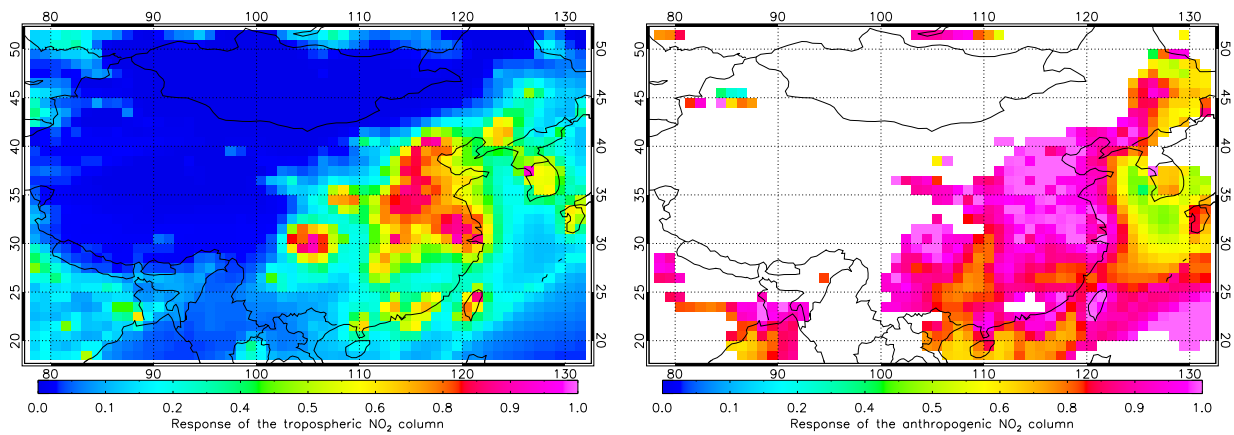


Figure 6.1: Left panel: Response of the tropospheric NO₂ column for every $1 \times 1^\circ$ grid cell on emissions with EMF=2 and EMF=1, respectively. Right panel: Response of the anthropogenic NO₂ column for every $1 \times 1^\circ$ grid cell on emissions with EMF=2 and EMF=1, respectively. For the white grid cells the response is undefined, since no or only very small anthropogenic emissions are present.

To get the response from only the anthropogenic emissions, only grid cells that are dominated by anthropogenic emissions are included. To find these grid cells, we took the month of maximum NO₂ concentration as a selection criterion. The month of maximum NO₂ has been determined by *van der A et al.* (2006a). A comparison for the month of maximum NO₂ for satellite observations and simulations will be discussed in chapter 9. As explained in section 3.1, grid cells with a maximum NO₂ in the winter are dominated by anthropogenic emissions. Therefore, only grid cells that have a maximum in NO₂ column in December, January or February are included. The grid cells that do not have a winter

maximum in NO_2 are shown in white in the right panel of figure 6.1 and will be excluded from the analysis. If anthropogenic NO_x emissions at these grid cells are present, we will not rescale them in this top-down inventory. For the included grid cells, we account for the contribution from natural emissions to the response by performing an extra model simulation with $\text{EMF}=0$. The resulting tropospheric column only contains NO_2 from natural sources, referred to as the natural column. Subtracting the natural column from all the other simulated tropospheric NO_2 columns gives a column that only contains NO_2 from anthropogenic sources. Therefore we refer to this column as the anthropogenic column. The response figure when comparing the anthropogenic columns for $\text{EMF}=2$ and $\text{EMF}=1$ is shown in the right panel of figure 6.1. The figure shows a response close to 1 for most areas. However, at some places at sea near the coastline the response is significantly lower, mainly in the waters around Korea. The reason for the lower response in this area is unclear. Possibly these areas are falsely attributed to regions dominated by anthropogenic emissions. Also persistent enhanced removal of NO_2 could cause the low response. Either way, this phenomenon is beyond the scope of this study.

The response of the anthropogenic NO_2 column is equal to approximately 1 for pixels over land that are dominated by anthropogenic emissions. The response of the anthropogenic NO_2 column on other EMF 's is equivalent. For a constant response of 1 in the anthropogenic NO_2 column (independent of the anthropogenic NO_x emissions) Ω_{ant} (6.1) can be rewritten as

$$\frac{\Omega_{ant,1}}{E_{ant,1}} = \frac{\Omega_{ant,2}}{E_{ant,2}}, \quad (6.2)$$

which is equivalent to a linear relation between anthropogenic NO_2 column and anthropogenic NO_x emission.

6.2 Approximate linearity

To describe the linear relation between the yearly averaged anthropogenic NO_2 column Ω_{ant} and the yearly anthropogenic NO_x emission E_{ant} , we introduce the parameter α , defined by

$$\Omega_{ant} = \alpha E_{ant}, \quad (6.3)$$

The parameter α is assumed constant for every grid cell, but a wide variation in α along grid cells is found. Since the typical size of a grid cell at $1 \times 1^\circ$ resolution over China is ~ 100 km, transport of NO_x to neighbouring grid cells is an important factor despite its short lifetime. NO_x from a source in a particular grid cell is spread out over its neighbouring grid cells, affecting the relation between the local emission and local column. The impact of NO_x transport on the local α is most pronounced in regions with high gradients in tropospheric NO_2 . Examples for a few grid cells are shown in figure 6.2. The figure shows the anthropogenic NO_x emissions E_{ant} and corresponding anthropogenic NO_2 column Ω_{ant} for the simulations with $\text{EMF}=1, 1.5, 2, 4, 6$ and 8 and a linear fit to the data points for every grid cell. Note the wide range in values of α that is found.

The linear coefficient α relates the anthropogenic NO_2 concentrations to anthropogenic

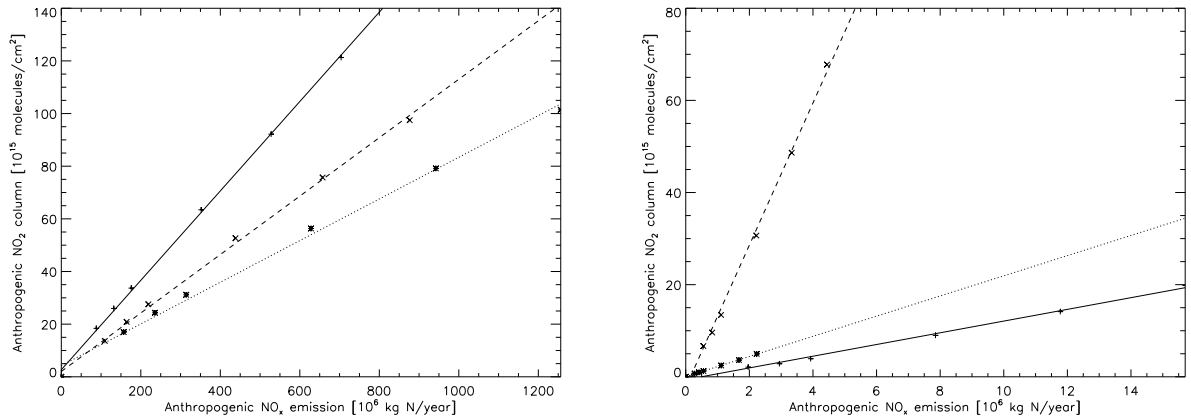


Figure 6.2: The anthropogenic NO₂ column plotted against anthropogenic NO_x emissions for a selection of 6 grid cells. The left panel shows the relation for Beijing (+), Shanghai (*) and Taipei (×). The linear fit for these three cities is represented by the solid, dotted and dashed line, respectively. The right panel shows this relation for grid cells in rural areas. Their locations are given by (longitude,latitude) = (110.5, 32.5), (108.5, 26.5) and (113.5, 32.5). These three grid cells are represented by the + symbol and dashed line, * symbol and dotted line and × symbol and dashed line, respectively.

NO_x emissions. According to *Martin et al.* (2003), it can be written as

$$\alpha = \frac{\Omega_{\text{NO}_2}}{\Omega_{\text{NO}_x}} \tau_{\text{NO}_x}, \quad (6.4)$$

where $\Omega_{\text{NO}_2}/\Omega_{\text{NO}_x}$ represents the ratio of local tropospheric NO₂ and NO_x columns, and τ_{NO_x} is the effective lifetime of anthropogenic NO_x in the troposphere.

6.3 A first top-down estimate

Using the parameter α from the previous section and the yearly averaged SCIAMACHY NO₂ column observations for 2003, the anthropogenic NO_x emission from the top-down estimate E_{td} is determined for every 1×1° grid cell. First, the natural column Ω_{nat} is subtracted from the tropospheric NO₂ column Ω_{obs} , thus obtaining an estimate of the anthropogenic NO₂ column measured by satellite. This means E_{td} can be written as:

$$E_{td} = \frac{\Omega_{obs} - \Omega_{nat}}{\alpha}. \quad (6.5)$$

To check the new anthropogenic NO_x emission database, we have simulated the year 2003 using these emissions. Figure 6.3 shows the yearly averaged tropospheric NO₂ column for 2003 measured by SCIAMACHY, the simulated tropospheric NO₂ column and the difference between these two. There are large differences between the observed and simulated tropospheric NO₂ column. For most of Eastern China simulated tropospheric NO₂ columns are smaller than the observed columns. However, for some grid cells the TM5 result exceeds the observed tropospheric NO₂ column, which is most significant in Korea. The most

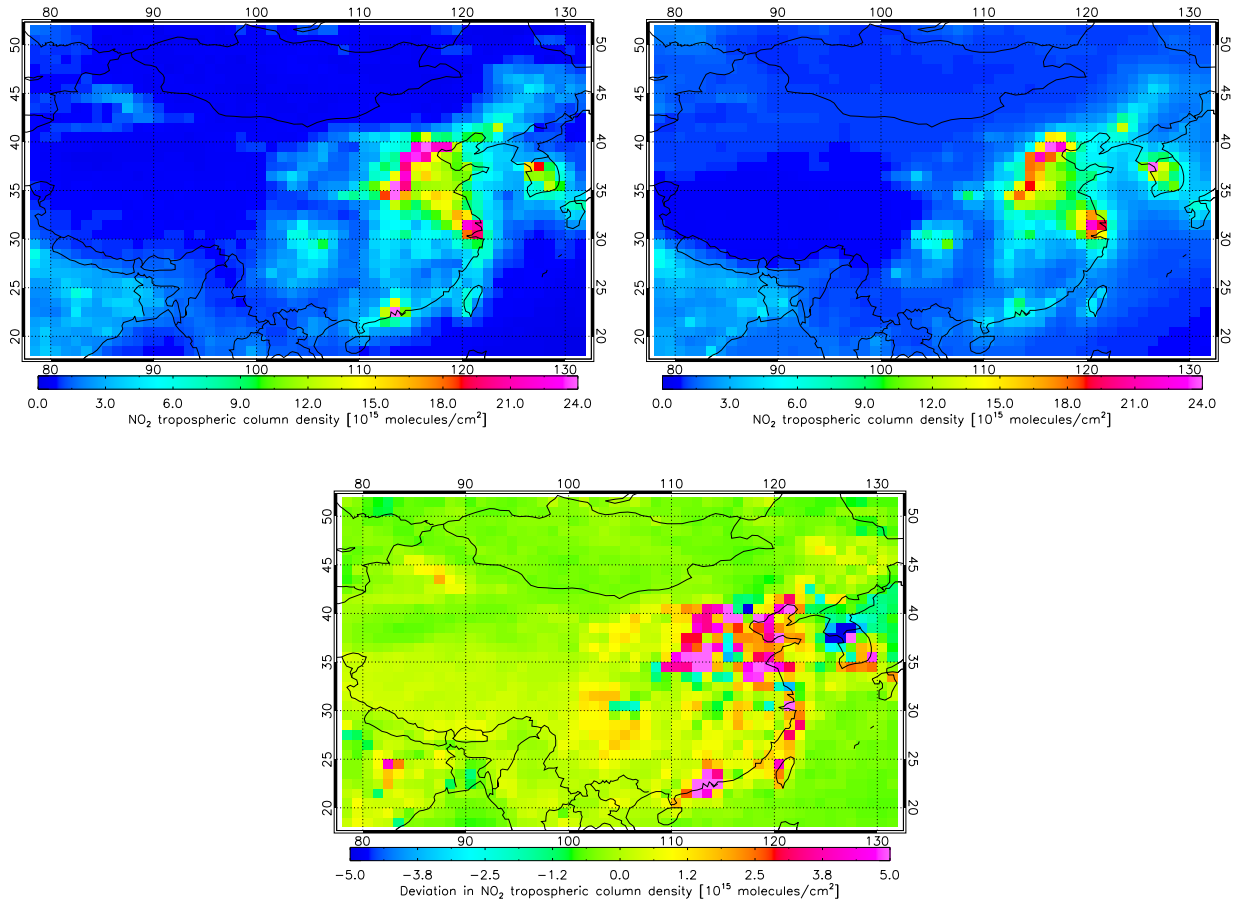


Figure 6.3: Yearly averaged tropospheric NO₂ columns for 2003, measured by SCIAMACHY (top left panel) and simulated using TM5 (top right panel). Anthropogenic NO_x emissions for the model are provided by the a posteriori emission database. The bottom panel shows the difference between the two top figures.

important process causing these differences is the non-uniform rescaling that has been applied to the anthropogenic NO_x emissions (with respect to EDGAR 3.2 anthropogenic NO_x emissions). As a result the amount of NO_x transport between grid cells changes, which affects the parameter α , relating the local emission and column.

So far we have followed the approach by *Martin et al.* (2003). They performed a global top-down inventory based on GOME retrievals for the year 2000. Between column and emission they assumed a linear relation based on mass conservation. They did one simulation with *a priori* emissions to find the linear coefficient α . In section 6.1 we have confirmed this linear relation by simulating for a wide range of anthropogenic NO_x emissions. Similar to what the procedure in this section, *Martin et al.* (2003) used the parameter α together with the retrieved tropospheric NO₂ columns from GOME to estimate the anthropogenic NO_x emissions. However, figure 6.3 shows that still significant differences between simulated and observed tropospheric NO₂ columns are present after this inversion, due to the non-uniform rescaling of the anthropogenic NO_x emissions. In the next section an iterative

procedure will be presented to improve the estimates for the anthropogenic NO_x emissions.

6.4 Iterative procedure

To improve our anthropogenic NO_x emission estimates, an iterative procedure will be used. From the latest simulation we can define a new α as the ratio of the simulated anthropogenic NO₂ column Ω_{ant} and the top-down emissions E_{td} . Again the anthropogenic NO₂ column is found by subtracting the natural NO₂ column from the simulated tropospheric NO₂ column. The new α is then used to re-estimate the anthropogenic NO_x emissions based on the observed tropospheric NO₂ columns by SCIAMACHY, according to (6.5). Subsequently, the newest anthropogenic NO_x emissions can be checked again by using them in a simulation. Still significant differences exist between observed and simulated tropospheric NO₂ columns, but differences have generally decreased.

This iterative process is repeated until the difference between the simulated and observed tropospheric NO₂ columns is less than 5%. In this case the iteration has been repeated 4 times. The final results of this procedure are shown in the figures 6.4 and 6.5.

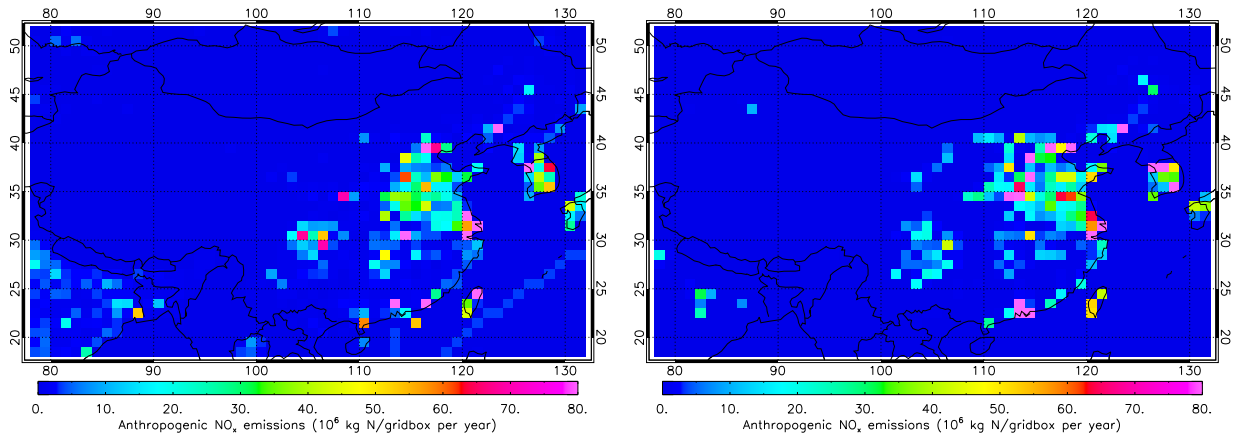


Figure 6.4: The anthropogenic NO_x emissions according to the EDGAR 3.2 database (left panel) and the final emission database from the top-down inventory for 2003 described in this chapter (right panel).

Figure 6.4 shows increased anthropogenic NO_x emissions around Beijing and Hong Kong and in the city of Urumqi, in the northwest of China. Also, higher anthropogenic NO_x emissions around the Yellow River can be seen. On the contrary, anthropogenic NO_x emissions around Chengdu and Chongqing have been decreased. Ship track emissions east of China have disappeared in the new emission estimate. The estimated total of anthropogenic NO_x emissions in China in 2003 is 4.33 Tg N, a 31% increase with respect to the anthropogenic NO_x emissions from EDGAR 3.2. Figure 6.5 shows that the differences between simulations and observations have decreased since the first estimate in section 6.3. Differences are still found; model overestimations are compensated by underestimations elsewhere. The differences are most pronounced in areas with high gradients in tropospheric NO₂, such as

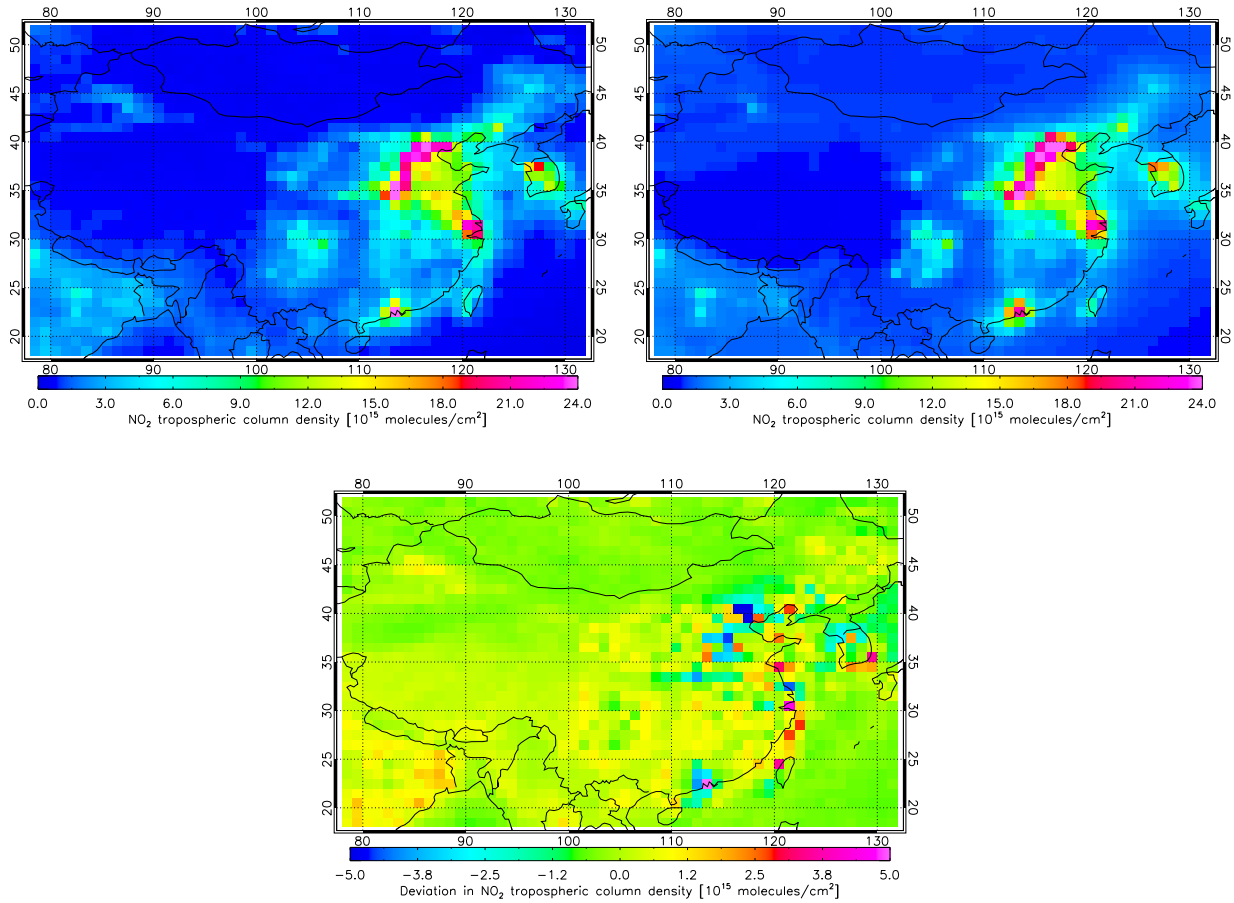


Figure 6.5: Yearly averaged tropospheric NO₂ columns for 2003, measured by SCIAMACHY (top left panel) and simulated using TM5 (top right panel). Anthropogenic NO_x emissions for the model are provided by the final emission database (right panel of figure 6.4). The bottom panel shows the difference between the two top figures.

the coastline, around Hong Kong and north of Beijing. The high gradients are not always resolved in the satellite observations, especially for GOME.

6.5 Discussion

By matching the simulated to observed tropospheric columns, the GOME and SCIAMACHY retrievals are expected to represent the true NO₂ tropospheric column. However, *van Noije et al.* (2006) find significant differences between different retrieval methods for GOME retrievals for the year 2000. It is found that over Eastern China retrievals of KNMI & BIRA-IASB (used in this study) significantly exceed retrievals by other groups. This difference is most significant in winter. If the retrievals used in this study are too high, the emission estimates for anthropogenic NO_x will be too high as well. Furthermore, it is found that over industrialized areas on average the models underestimate the retrievals,

particularly over Eastern China. The difference over Beijing is $6.0 \cdot 10^{15}$ molecules cm^{-2} and can be explained by underestimated NO_x emissions in Eastern China. These differences are more pronounced in winter, indicating that winter NO_x emissions are higher than summer NO_x emissions.

7

Growing NO_x emissions in China

A similar procedure as described in chapter 6 can be used to estimate anthropogenic NO_x emissions for other years as well. With the new top-down estimates for the emissions the observed growth in tropospheric NO₂ columns can be related to increase in anthropogenic NO_x emissions. In this chapter we will estimate the anthropogenic NO_x emissions for the years 1997-2005 (except 2003) and compare the trend in anthropogenic NO_x emissions to the observed trend in tropospheric NO₂ columns. However, in this chapter we apply a slightly modified procedure that uses the observed trend in tropospheric NO₂. This approach is described below.

7.1 Emission estimates for other years

For the *a priori* estimate of the anthropogenic NO_x emissions of an arbitrary year y , we use the top-down estimates for 2003 in a linear model, where the trend in tropospheric NO₂ [*van der A et al.* (2006a)] is used. The *a priori* anthropogenic NO_x emission for every grid cell is defined as

$$E(y) = E_0 + \alpha T(y - 2003), \quad (7.1)$$

where E_0 is the local anthropogenic emission in 2003, T represents the local trend in NO₂ tropospheric columns and α describes the relation between local anthropogenic NO_x emission and local anthropogenic NO₂ column. All these parameters are supplied for each year and for every grid cell individually. Both E_0 and α are determined by the inversion procedure described in chapter 6, while T is constructed from satellite data by *van der A et al.* (2006a). The advantage of this *a priori* estimate over the EDGAR 3.2 database is that it is expected to be close to the top-down estimate. This will reduce the number of iterations necessary to determine the top-down emissions in this chapter.

Tropospheric NO₂ columns are simulated using *a priori* emissions from (7.1). Comparing the simulated columns to the retrieved columns from the satellite resulted in deviations again. In a second simulation these differences are used to rescale the emissions, equivalent to the procedure described in chapter 6. Only one correction of the *a priori* is needed to scale the emissions.

This procedure has been followed for all the years between 1997 and 2005 (except for 2003).

7.2 Annual emission trends

The resulting 9-year dataset has been fitted to a linear trend model, described by

$$E(y) = \beta y + \gamma, \quad (7.2)$$

where E represents the local emission strength, y is time in years, β the local trend in the anthropogenic NO_x emissions and γ the offset in anthropogenic NO_x emissions. The spatial distribution of the trend β is shown in figure 7.1. This figure also contains the trend in tropospheric NO₂ measured by satellite. To obtain this trend, yearly averaged tropospheric NO₂ columns for the period 1997-2005 have been fitted to a linear trend model. The figure shows that the growth in anthropogenic NO_x emissions is mainly found in China's major cities, while the observed trend in NO₂ is found over a large area in East China. The trend in emissions is more localized than the trend in tropospheric NO₂.

The largest trend in anthropogenic NO_x emissions is found over major cities such as Beijing, Shanghai, Zhengzhou, Hangzhou and the Pearl River Delta¹. Trend values for individual cities in China are shown in table 7.1. This table also contains the relative trend in NO₂ tropospheric columns based on 1997, calculated from yearly averaged tropospheric NO₂ columns over the same time period 1997-2005. The bottom row of the table shows the total of anthropogenic NO_x emissions in China and its trend.

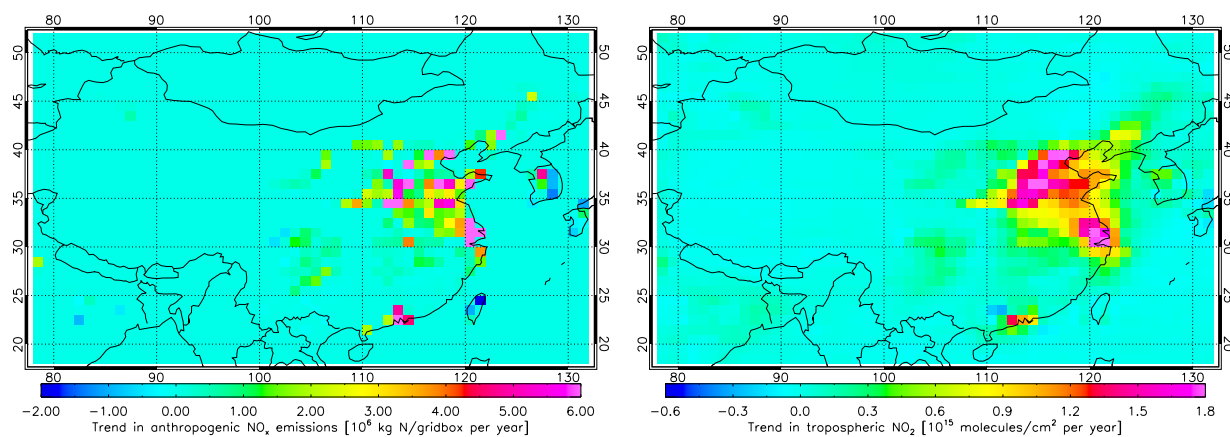


Figure 7.1: Left panel: yearly increase in anthropogenic NO_x emissions. Right panel: yearly increase in tropospheric NO₂ columns measured by satellite. Both trends are based on the linear trend model for the time period 1997-2005.

Table 7.1 shows that for most major cities the trend in NO_x emissions is slightly higher than the trend in columns. This is explained by the fact that NO_x is transported from grid cells with a large yearly increase in anthropogenic NO_x emissions to their neighbouring

¹The Pearl River Delta is the bay between the cities of Hong Kong, Macao and Guangzhou

City	1997	Absolute trend	Relative trend	Observed relative trend
PR Delta	163	20.7 ± 5.4	$13 \pm 3 \%$	$9 \pm 2 \%$
Beijing	147	25.1 ± 5.8	$17 \pm 4 \%$	$14 \pm 2 \%$
Shanghai	133	35.9 ± 5.4	$27 \pm 4 \%$	$23 \pm 3 \%$
Taipei	71	-4.5 ± 1.3	$-6 \pm 2 \%$	$0 \pm 2 \%$
Shenyang	58	13.8 ± 2.1	$24 \pm 4 \%$	$19 \pm 3 \%$
Harbin	26	2.2 ± 1.0	$9 \pm 4 \%$	$9 \pm 3 \%$
Chongqing	25	0.7 ± 0.6	$3 \pm 2 \%$	$6 \pm 2 \%$
Xi'An	21	1.9 ± 0.8	$9 \pm 4 \%$	$20 \pm 5 \%$
Jinan	17	3.8 ± 0.7	$22 \pm 4 \%$	$18 \pm 3 \%$
Chengdu	14	1.1 ± 0.2	$8 \pm 1 \%$	$8 \pm 1 \%$
Urumqi	9	0.6 ± 0.3	$7 \pm 4 \%$	$4 \pm 2 \%$
China total	2673	401 ± 54	$15 \pm 2 \%$	

Table 7.1: Anthropogenic NO_x emissions and their trends for cities throughout China. Emissions are given in 10^6 kg N per year. Relative trends are based on the linear trend model, with 1997 as reference year. For comparison, the last column contains the relative trend in observed NO_2 tropospheric columns (from GOME and SCIAMACHY).

grid cells. Therefore, the relative trend in NO_x emissions is higher than the relative trend in tropospheric NO_2 in these grid cells. Subsequently, the relative trend in NO_x emissions is lower than the trend in tropospheric NO_2 columns in their neighbouring grid cells. Significant differences between the trends in emissions and columns are found in Xi'An and Taipei. For Taipei, a significant decrease in anthropogenic NO_x emissions is found, while the NO_2 columns do not show a trend. For Xi'An, the increase in anthropogenic NO_x emissions is much smaller than the increase in tropospheric NO_2 from satellite observations. This might be explained by the large increase in tropospheric NO_2 in 2005 compared to the years before, which is not represented in the emission after one emission correction. Figure 7.2 shows the yearly NO_x emissions for Beijing, Shanghai and the Pearl River Delta, as well as the countries total emissions of NO_x . The total is calculated by adding all anthropogenic NO_x emissions from grid cells within the borders of China (Taiwan is not included). The solid line represents the linear fit that was determined for every grid cell. In the top left figure (Beijing) a jump in the emission strength is seen from 2002 to 2003, at the time that the switch between GOME and SCIAMACHY was made. Because Beijing is at the edge of the polluted region of East China, the low-resolution GOME pixels also cover a part of the less polluted area north of the city, while for SCIAMACHY this is not the case.

In all four figures the trend in NO_x emissions is accelerating in the latter years of our time period, due to the increasing trend in tropospheric NO_2 . To account for the increasing trend in emissions, an exponential model has also been fitted to the data, represented by the dashed lines in figure 7.2. This exponential trend model is represented by

$$E(y) = A + Be^{Cy} \quad (7.3)$$

where $E(y)$ is the emission strength for an arbitrary year y and A , B and C are the fit

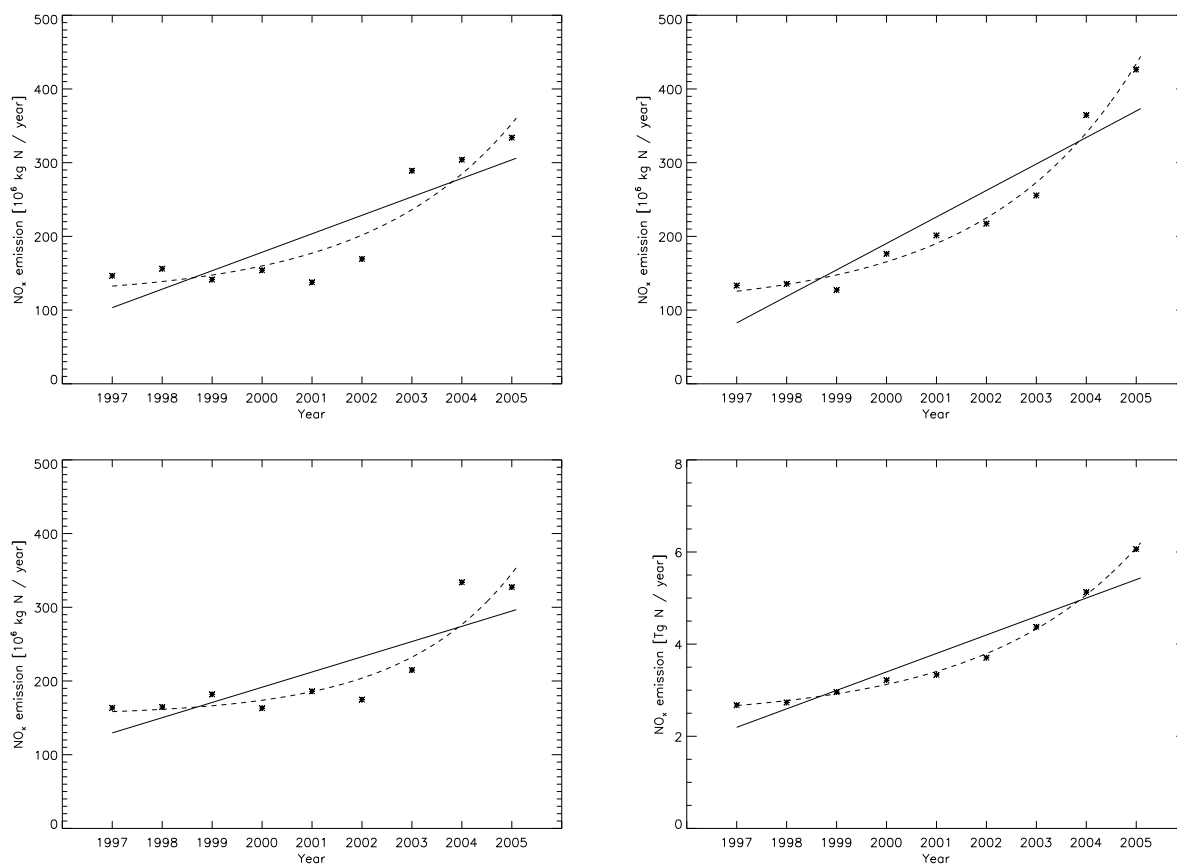


Figure 7.2: Time series of anthropogenic NO_x emissions for the years 1997-2005 in Beijing (top left panel), Shanghai (top right), the Pearl River Delta (bottom left) and in China as a whole (bottom right panel).

parameters. As can be seen in figure 7.2, the exponential model conforms better to the emissions found, especially when we consider the sum of all anthropogenic NO_x emissions in China. For this model, the growth in emissions in China increases from 4% for 1998 to 20% for 2005, where the percentage is based on the year before.

7.3 Global implications

As pointed out in section 2.2, changing NO_2 concentrations affect the ozone concentrations. Clearly these large increases will have severe consequences for the local air quality, but even effects on the global scale can be expected, because the lifetime of tropospheric ozone is much larger than the lifetime of NO_2 . In addition, PAN formation will contribute to the global impact of the increased emissions.

To study the changes in global tropospheric ozone concentrations caused by changing NO_2 over China, two simulations for 2005 are compared. The first simulation uses our top-down estimate for the anthropogenic NO_x emissions for 2005, while the second uses our top-

down estimate for 1997, assuming zero growth. For both cases yearly averaged tropospheric ozone columns, as well as surface ozone concentrations, are calculated from the model results. By subtracting one from the other, the difference in global tropospheric ozone caused by the increasing Chinese emissions over the time period 1997-2005 is obtained. Figure 7.3 shows the difference in surface ozone and ozone tropospheric column. The figure shows that ozone concentrations have increased on the entire Northern Hemisphere, due to the increased emissions over China. However, for ground level ozone a decrease in China itself is observed, caused by changes in the chemical regime. We find an increase of 0.4% in global tropospheric ozone, which is a result from the increasing anthropogenic NO_x emissions in China between 1997 and 2005. For the USA the increase in tropospheric ozone is 0.8%, for Europe 0.5%. Because the main winds are from the west, ozone is flowing eastward and changes in ozone concentration outside China are most pronounced over the Pacific ocean. Over land, ozone is removed from the troposphere by deposition and changes are less pronounced than over sea. This can clearly be seen over North America.

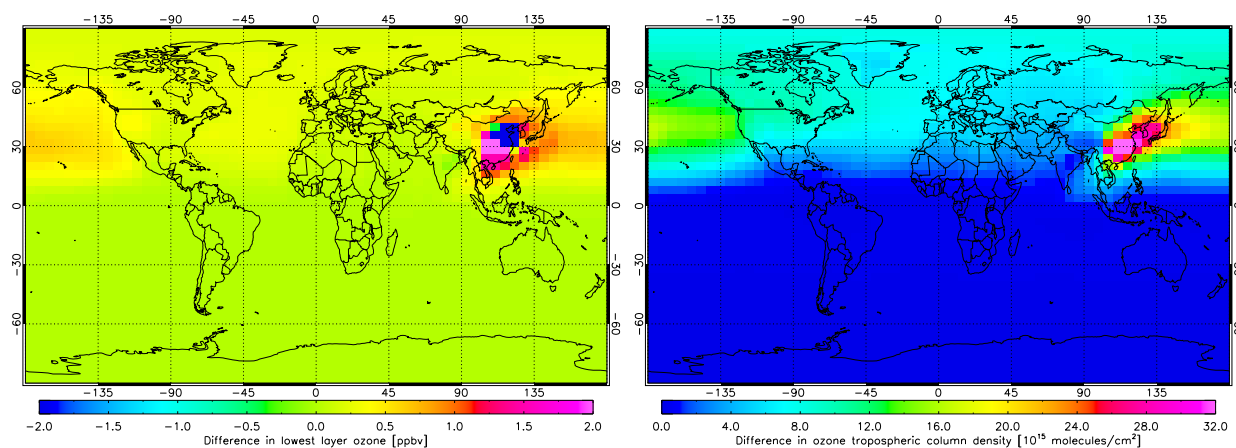


Figure 7.3: Left panel: The difference in ground-level ozone caused by the increase of Chinese NO_x emissions between 1997 and 2005. Right panel: The increase in tropospheric ozone columns caused by the increase of Chinese NO_x emissions between 1997 and 2005.

Nitrogen oxides can be transported over long distances if transformed into PAN, as described in chapter 2. The two simulations for 2005, with 2005 and 1997 emissions, respectively, can be used to see changes in the global PAN tropospheric column density due to the increasing emissions over China. This difference is shown in figure 7.4. As expected, the results show increasing PAN concentrations over the entire Northern Hemisphere, particularly over the Pacific.

Tropospheric ozone is a strong greenhouse gas. The model results clearly indicate that large increases in NO_x emissions not only affect the local air quality but also contribute to climate change.

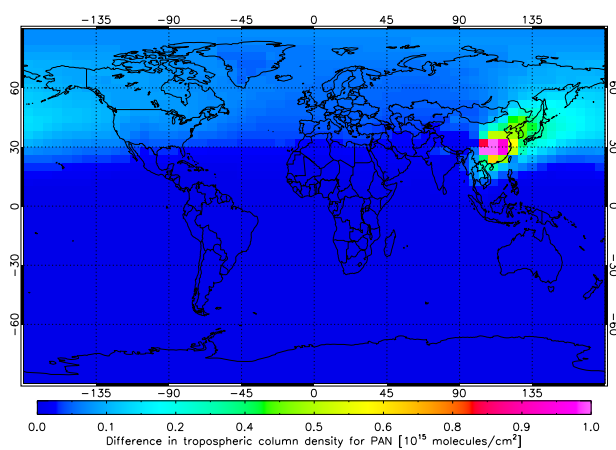


Figure 7.4: The increase in PAN tropospheric column between 1997 and 2005, because of increasing anthropogenic NO_x emissions in China only.

8

Comparison to previous inventories

Multiple emission inventories for NO_x emissions in China have been constructed in the past, most of them based on energy consumption forecasts and statistical data (bottom-up inventories). In this section, these emission estimates within the time range 1997-2005 will be compared to the top-down results of our study.

- In the EDGAR database [*Olivier and Berdowski (2001)*], the total of anthropogenic NO_x emissions in China equals 3.3 Tg N, based on the year 1997.
- *Van Aardenne et al. (1999)* present an anthropogenic emission inventory for Asia for the period 1990-2020. The NO_x emissions in China are based on the RAINS-ASIA methodology, which includes a dynamic model for energy forecasts. The total of NO_x emissions in China for 1990 is estimated to be 2.5 Tg N, while their estimates for 2000, 2010 and 2020 are 4.2, 6.7 and 9.9 Tg N, respectively. This indicates an accelerating trend in NO_x emissions, which is also seen in our emission estimates. However, their estimate for 2000 is higher than our estimate for this year, which is 3.2 Tg N. This might be caused by the fact that they included emissions from biomass burning and biofuels. In our inventory, only anthropogenic NO_x emissions from fossil fuel combustion and industrial activities are taken into account.
- *Streets et al. (2003)* present an inventory of air pollutant emissions in Asia for the year 2000. The estimated total of yearly NO_x emissions for Asia is 8.2 Tg N, for China only 3.5 Tg N, around 10% higher than our estimate.
- *Hao et al. (2002)* find a rapid increase in NO_x emissions from 1.4 Tg N in 1980 to 3.7 Tg N in 1996, but a small decrease of 0.11 and 0.26 Tg N for 1997 and 1998, respectively. In the latter study, only emissions from commercial energy consumption are included. This decrease is not found in our analysis.
- *Streets and Waldhoff (2000)* estimate emissions for 29 different regions of China, also using the RAINS-ASIA simulation model. Data for 1990 and 1995, as well as two projections for the year 2020 are presented. They find 2.9 and 3.7 Tg N as China total anthropogenic emissions for 1990 and 1995, respectively. This increase is mainly due to the increase in emissions from transportation (62%), while industrial,

power and domestic emissions all increased by 20%. Despite the large growth of the transportation sector, the industry and power generation sectors still account for more than 75% of the total NO_x emissions. For 2020, they find an estimated total NO_x emissions in China of 8.1-9.0 Tg N.

- *Wang et al.* (2005) present a high-resolution emission inventory for eastern China in 2000. Projected is a huge increase in emissions if no measures are taken by the Chinese government. NO_x emissions are expected to increase by 130-250% from 2000 to 2020.
- *Wang et al.* (2004) use observations from the Transport and Chemical Evolution over the Pacific (TRACE-P) aircraft mission over the northwest Pacific in 2001 and data from two Chinese ground stations, in combination with an inverse modelling setup, to estimate emissions of NO_x and CO in Asia. For China, they find a total emission of 5.0 Tg N per year.
- *Martin et al.* (2003) performed a top-down NO_x inventory based on GOME retrievals for the year 2000. For East Asia (China and Korea), they find a total of 4.7 Tg N. This total includes emissions from biomass burning and biofuel, as well as natural emissions. Our method can be regarded as an adapted version of that of *Martin et al.* (2003) for anthropogenic NO_x , as discussed in chapter 6.
- *Jaeglé et al.* (2005) performed a top-down inventory for NO_2 based on GOME for the year 2000. Their estimate for the a posteriori NO_x emissions from fossil fuel combustion for China is 4.4 Tg N per year, significantly more than found in our top-down inventory.

Table 8.1 contains the sum of all anthropogenic NO_x emissions for China from the different inventories.

Study	Type	Emission
This study	top-down	3.2
<i>Van Aardenne et al.</i> (1999)	bottom-up	4.2
<i>Streets et al.</i> (2003)	bottom-up	3.5
<i>Wang et al.</i> (2004)	top-down	5.0
<i>Martin et al.</i> (2003)	top-down	4.7
<i>Jaeglé et al.</i> (2005)	top-down	4.4

Table 8.1: Comparison between total anthropogenic NO_x emissions found for China from different inventories. Emissions are in Tg N per year. All estimates are given for the year 2000.

All the inventories described in this study find larger NO_x emissions than our top-down inventory for the year 2000. Possible causes for these differences are the fact that we only take the emissions from grid cells within the Chinese borders, while other top-down

inventories might add all emissions from a larger area, perhaps including Korea or cities in South or Southeast Asia. A second reason is the fact that we only take emissions from fossil fuel combustion and industrial activities, while other studies often also take NO_x from biomass burning into account. In this study we have assumed that the increase in tropospheric NO_2 is accounted for by growing anthropogenic NO_x emissions from fossil fuel combustion and industrial activity only. Therefore, NO_x emissions from biofuel are not taken into account in this study. According to table 5.1, emissions from biofuel account for a total of 0.44 Tg N per year.

9

Seasonal variation in NO₂ columns

NO₂ concentrations are different for every season. The driving force for this variability is the changing amount of sunlight, as explained in section 3.1. Using the results from the simulations for the years 1997-2005 from chapter 7, the modelled seasonal cycle can be determined. For comparison to the satellite observations, simulated tropospheric NO₂ columns are taken at satellite overpass time, as described in section 5.3.

For every month, an average tropospheric NO₂ column has been calculated for the 9-year dataset 1997-2005. The seasonal cycle in the NO₂ column T for every grid cell can be represented by the function

$$T = A + B \sin[\Omega(t + \phi)], \quad (9.1)$$

where A represents the average NO₂ column, B the amplitude of the oscillation, Ω the frequency of the oscillation, t the time in months and ϕ the phase shift. In our case, the frequency Ω of the oscillation is fixed to one year and the parameters A , B and ϕ are determined by fitting the 12 monthly averaged NO₂ columns to this model. The month of maximum NO₂ concentration is given by

$$t_{max} = \begin{cases} \frac{3\pi}{2\Omega} - \phi, & B < 0, \\ \frac{\pi}{2\Omega} - \phi, & B > 0. \end{cases} \quad (9.2)$$

A fixed frequency of 12 months yields $\Omega = \pi/6$, and the month of maximum NO₂ concentration is given by $t_{max} = 3 - \phi$ (for positive amplitude B). The season of maximum NO₂ is determined from the month of maximum NO₂, where summer is represented by June, July and August, winter by December, January and February, etc. The season of maximum NO₂ is shown in figure 9.1, for both satellite observations and TM5 simulations between 1997 and 2005.

As expected, a winter maximum in NO₂ is found for most of Eastern China, but an inverse seasonal cycle, with a summer maximum, is found for various major cities such as Beijing, Shanghai and Hong Kong. The in situ measurements used in chapter 3 confirm to the satellite observations, showing a winter maximum (in the boundary layer). It is unclear why the model shows a summer maximum in NO₂ over China's major cities. Perhaps this is due to a change in the chemical regime. For most of Western China, simulations and observations both show a maximum in NO₂ in summer. Differences in the season of

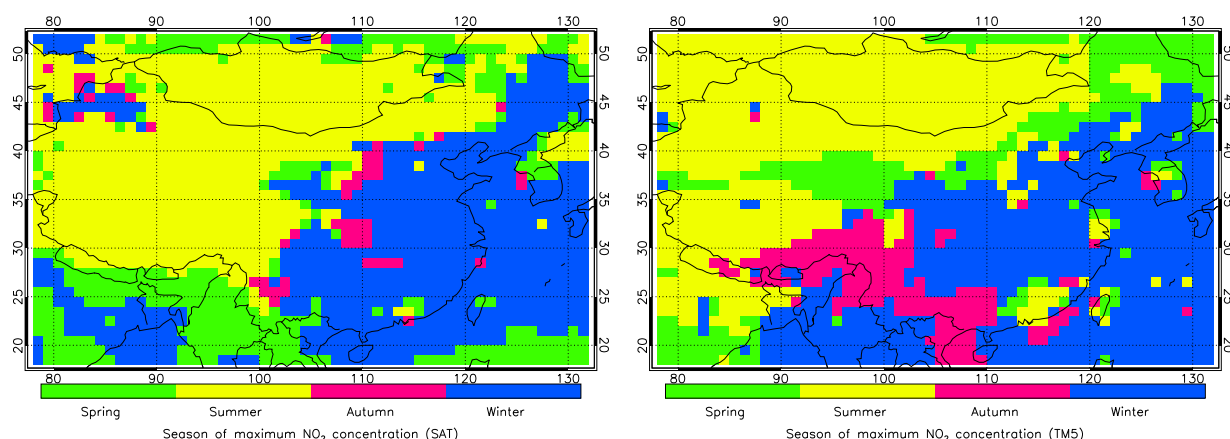


Figure 9.1: The month of maximum tropospheric NO₂ column, for the satellite retrievals (left panel) and simulated using TM5 (right panel). Data are averaged monthly means for the years 1997-2005.

maximum NO₂ are found in Central China, just south of China (India, Myanmar) and also in the northwest of China. In Western China, a summer maximum is found for most grid cells. This was also found from analysis of GOME & SCIAMACHY tropospheric NO₂ [van der A *et al.* (2006a)]. The summer maximum is due to higher soil NO_x emissions in this season, but also more lightning events are likely to contribute to higher NO₂ columns in summer.

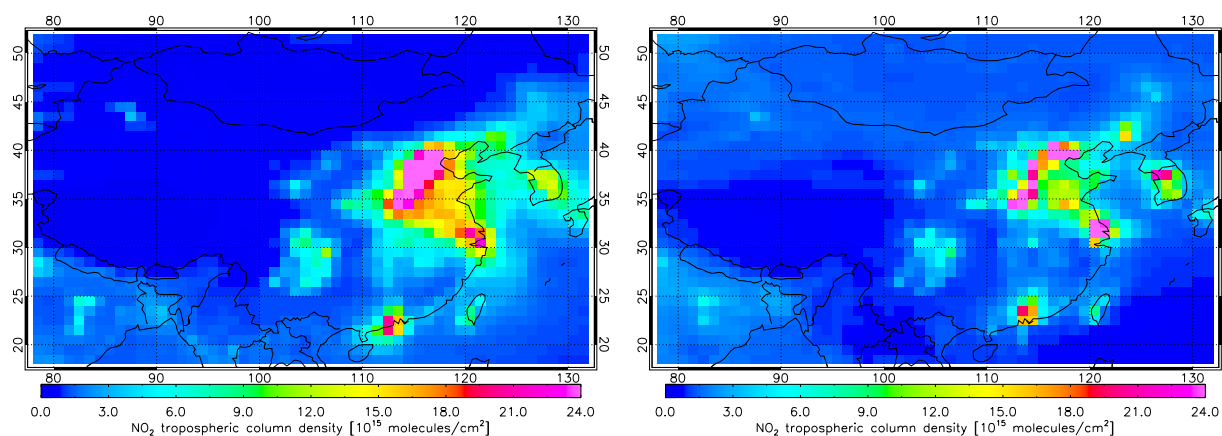


Figure 9.2: Simulated monthly averaged NO₂ concentrations for January 2003 (left panel) and July 2003 (right panel).

In figure 9.2 monthly mean tropospheric NO₂ columns are shown for January 2003 and July 2003. The figure shows that in winter tropospheric NO₂ columns are generally higher in Eastern China, however the NO₂ concentrations in some major cities are lower. Since anthropogenic NO_x emissions are the same, NO_x stays closer to its source in summer than in winter. Possible explanations may be faster removal of NO_x from the atmosphere in the summer, or different meteorological conditions for summer and winter. The seasonal

pattern in NO_2 can be used to determine the dominating NO_x emission in every single grid cell, based on the month of maximum NO_2 . This procedure is described in *van der A et al.* (2006b). This paper also compares the month of maximum NO_2 concentration found from satellite observations and from a model simulation.

10

Conclusions and outlook

In this study we have used satellite data of tropospheric NO_2 to construct an improved emission database for anthropogenic NO_x emissions for the 9-year period 1997-2005. First, the relation between emission and column has been determined using the chemistry-transport model TM5. A linear relation between the anthropogenic NO_x emission and anthropogenic NO_2 column has been found, but the linear coefficient α shows a large variation along grid cells. This is caused by NO_x transport between grid cells and is most pronounced in regions with large gradients in tropospheric NO_2 .

The linear relation can be used in combination with satellite observations of tropospheric NO_2 to estimate the anthropogenic NO_x emissions in China. The same approach has been used by *Martin et al.* (2003). However, a simulation with these new emissions shows large differences with the observed tropospheric NO_2 columns. Because we have applied a non-uniform rescaling to the NO_x emissions, transport of NO_x between grid cells will change, affecting the linear coefficient α . From the difference between simulated and observed tropospheric NO_2 columns, the anthropogenic NO_x emissions can be re-estimated. After running 4 iterations, the difference between simulated and observed tropospheric NO_2 columns is within 5%.

When comparing the emissions from our top-down inventory to the emissions from EDGAR 3.2, significant differences are found. Emissions in the cities in East-China (around Beijing and Shanghai), as well as the emissions around Hong Kong are higher in our inventory. On the contrary, NO_x emissions around Chongqing have been scaled down in our inventory. The total of NO_x emissions in China in 2003 has increased from 3.3 Tg N (EDGAR) to 4.3 Tg N in our top-down inventory.

By running the inversion for all the years in the time period 1997-2005, the trend in emissions can be determined. As expected, the highest trends in anthropogenic NO_x emissions are found where the highest trends in tropospheric NO_2 are detected. The yearly increase in NO_x emissions in Shanghai is 27% and in Beijing 17%, while the total of NO_x emissions in China increases by 15% every year (compared to the 1997 emission).

The inversion procedure has been applied for China, but it can be applied to the whole world in the future. Unfortunately, computational limitations do not allow us to solve the whole world at a $1 \times 1^\circ$ resolution, but other specific regions of interest can be examined in detail using the zoom option of TM5.

Seasonal variations in NO_2 are found by the model, but do not agree everywhere with the satellite observations. This is likely to be due to the fact that most NO_x emissions in the model are constant throughout the year. Future comparisons between model and satellite observations can be used to find seasonal variations in anthropogenic NO_x emissions in East China. The same comparison can be made for the weekly cycle: emissions are expected to be less in the weekend, but this reduction is not present in the model yet. The difference between model and satellite observations is a measure for the changes in NO_x emissions. For future research, NO_2 data from SCIAMACHY, OMI (Ozone Monitoring Instrument) and GOME-2 can be used. The advantage of OMI observations is a higher spatial resolution and the ability to produce daily global maps of tropospheric NO_2 . The GOME-2 instrument is to be launched in July 2006. Since all instruments have a different overpass time, it is possible to find the diurnal behaviour of e.g. NO_2 .

Acknowledgements

I want to thank to Ronald van der A and Ernst Meijer, my supervisors at KNMI, for their help and support during the time I was conducting my research. Their advice and remarks have been very useful. I also want to thank my advisor Hennie Kelder, PI of the AMFIC air quality project, for the opportunity to conduct this research at KNMI.

Further, I would like to thank all people of AS (Atmospheric Composition) for their interest, assistance and kind cooperation. I want to mention a few people in particular: Arjo Segers, who was always ready to help me with model-related problems and Twan van Noije for the helpful discussions about NO₂.

I am very grateful that I had the opportunity to visit NSMC in Beijing in March 2006. Furthermore, I have attended the 2005 DRAGON symposium in Santorini and will attend the 2006 DRAGON symposium in July 2006. These 3 visits are financially supported by ESA.

References

- van der A, R. J., D. H. M. U. Peters, H. Eskes, K. F. Boersma, M. Van Roozendael, I. De Smedt, and H. M. Kelder, Detection of the trend and seasonal variation in tropospheric NO₂ over China, *J. Geophys. Res.*, in press, 2006a.
- van der A, R. J., H. Eskes, K. F. Boersma, T. P. C. van Noije, M. Van Roozendael, I. De Smedt, D. H. M. U. Peters, J. J. P. Kuenen, E. W. Meijer, and H. M. Kelder, Identification of NO₂ sources and their trends from space using seasonal variability analysis, *J. Geophys. Res.*, submitted, 2006b.
- van Aardenne, J. A., G. R. Carmichael, H. Levy, D. Streets, and L. Hordijk, Anthropogenic NO_x emissions in Asia in the period 1990-2020, *Atmos. Environ.*, *33*, 633–646, 1999.
- Beirle, S., U. Platt, M. Wenig, and T. Wagner, Weekly cycle of NO₂ by GOME measurements: a signature of anthropogenic sources, *Atmos. Chem. Phys.*, *3*, 2225–2232, 2003.
- Berkvens, P. J. F., M. A. Botchev, W. M. Lioen, and J. G. Verwer, A zooming technique for wind transport of air pollution, *Tech. Rep. MAS-R9921*, CWI, Amsterdam, 1999.
- Blond, N., K. F. Boersma, H. J. Eskes, R. J. van der A, M. Van Roozendael, I. De Smedt, G. Bergametti, and R. Vautard, Intercomparison of SCIAMACHY nitrogen dioxide observations, in-situ measurements and air quality modeling results over Western Europe, *J. Geophys. Res.*, in press, 2005.
- Boersma, K. F., H. J. Eskes, and E. J. Brinksma, Error analysis for tropospheric NO₂ retrieval from space, *J. Geophys. Res.*, *109*, D04311, doi:10.1029/2003JD003962, 2004.
- Boersma, K. F., H. J. Eskes, E. W. Meijer, and H. M. Kelder, Estimates of lightning NO_x production from GOME satellite observations, *Atmos. Chem. Phys. Discuss.*, *5*, 3047–3104, 2005.
- Bovensmann, H., J. P. Burrows, M. Buchwitz, J. Frerick, S. Noel, V. V. Rozanov, K. V. Chance, and A. P. H. Goede, SCIAMACHY: Mission Objectives and Measurement Modes, *J. Atmos. Sci.*, *56*, 127–150, 1999.
- Brasseur, G. P., J. J. Orlando, and G. S. Tyndall, *Atmospheric Chemistry and Global Change*, Oxford University Press, New York, 1999.

- Bucsela, E. J., E. A. Celarier, M. O. Wenig, J. F. Gleason, J. Veefkind, K. F. Boersma, and E. J. Brinksma, Algorithm for NO₂ vertical column retrieval from the ozone monitoring instrument, *IEEE Trans. Geo. Rem. Sens.*, in press, 2006.
- Burrows, J. P., M. Weber, M. Buchwitz, V. V. Rozanov, A. Ladstädter-Weissenmayer, A. Richter, R. de Beek, R. Hoogen, K. Bramstedt, and K. U. Eichmann, The Global Ozone Monitoring Experiment (GOME): Mission concept and first scientific results, *J. Atmos. Sci.*, *56*, 151–175, 1999.
- Dentener, F. J., and P. J. Crutzen, Reaction of N₂O₅ on tropospheric aerosols: impact on the global distributions of NO_x, O₃ and OH, *J. Geophys. Res.*, *98*(D4), 7149–7163, doi:10.1029/92JD02979, 1993.
- Dentener, F., W. Peters, M. Krol, M. van Weele, P. Bergamaschi, and J. Lelieveld, Interannual variability and trend of CH₄ lifetime as a measure for OH changes in the 1979-1993 time period, *J. Geophys. Res.*, *108*(D15), 4442, doi:10.1029/2002JD002916, 2003.
- ECMWF, *IFS documentation*, <http://www.ecmwf.int/research/ifsdocs/>, 2002.
- EPD, *Hong Kong Environmental Protection Department, Air Quality Monitoring Data*, <http://www.epd.gov.hk/epd/eindex.html>, 2005.
- Eskes, H. J., and K. F. Boersma, Averaging Kernels for DOAS total-column satellite retrievals, *Atmos. Chem. Phys.*, *3*, 1285–1291, 2003.
- Fortuin, J. P., and H. Kelder, An ozone climatology based on ozonesonde and satellite measurements, *J. Geophys. Res.*, *103*(D24), 31,709–31,734, doi:10.1029/1998JD200008, 1998.
- Ganzeveld, L., J. Lelieveld, and G.-J. Roelofs, A dry deposition parameterization for sulfur oxides in a chemistry and general circulation model, *J. Geophys. Res.*, *103*(D5), 5679–5694, doi:10.1029/97JD03077, 1998.
- Gardner, R., ANCAT/EC2 Global aircraft emissions inventories for 1991/92 and 2015, in *European Commission Directorate - General XI. Environment, Nuclear Safety and Soil Protection, and European Civil Aviation Conference*, 1998.
- Hao, J., H. Tian, and Y. Lu, Emission inventories of NO_x from commercial energy consumption in China, 1995-1998, *Environ. Sci. Technol.*, *36*, 552–560, 2002.
- Holtslag, A. A. M., and B. A. Boville, Local versus nonlocal boundary-layer diffusion in a global climate model, *J. Climate*, *6*, 1825–1842, 1993.
- Houweling, S., F. Dentener, and J. Lelieveld, The impact of nonmethane hydrocarbon compounds on tropospheric photochemistry, *J. Geophys. Res.*, *103*(D9), 10,673–10,696, doi:doi:10.1029/97JD03582, 1998.
- Jacob, D. J. J., *Introduction to atmospheric chemistry*, Princeton University Press, Princeton, New Jersey, 1999.

- Jaeglé, L., L. Steinberger, R. V. Martin, and K. Chance, Global partitioning of NO_x sources using satellite observations: Relative roles of fossil fuel combustion, biomass burning and soil emissions, *Faraday Discuss.*, *130*, 407–423, 2005.
- Junge, C. E., and P. E. Gustafson, On the distribution of sea salt over the United States and its removal by precipitation, *Tellus*, *9*, 164–173, 1957.
- Koelemeijer, R. B. A., J. F. de Haan, and P. Stammes, A database of spectral surface reflectivity in the range 335–772 nm derived from 5.5 years of GOME observations, *J. Geophys. Res.*, *108*(D2), 4070, doi:10.1029/2002JD002429, 2003.
- Krol, M., S. Houweling, B. Bregman, M. van den Broek, A. Segers, P. van Velthoven, W. Peters, F. Dentener, and P. Bergamaschi, The two-way nested global chemistry-transport zoom model TM5: algorithm and applications, *Atmos. Chem. Phys.*, *5*, 417–432, 2005.
- Langner, J., and H. Rodhe, A global three-dimensional model of the tropospheric sulfur cycle, *J. Atmos. Chem.*, *13*, 225–263, 1991.
- Lelieveld, J., and G. Helas, *Luchtverontreiniging in de troposfeer*, Meulenhoff Educatief BV, Amsterdam, 1987.
- Leue, C., M. Wenig, T. Wagner, O. Klimm, U. Platt, and B. Jähne, Quantitative analysis of NO_x emissions from Global Ozone Monitoring Instrument satellite image sequences, *J. Geophys. Res.*, *106*(D6), 5493–5506, doi:10.1029/2000JD900572, 2001.
- Logan, J. A., M. J. Prather, S. C. Wofsy, and M. B. McElroy, Tropospheric chemistry: a global perspective, *J. Geophys. Res.*, *86*(C8), 7210–7254, 1981.
- Martin, R. V., K. V. Chance, D. J. Jacob, T. P. Kursou, R. J. D. Spurr, E. Bucsela, J. F. Gleason, P. I. Palmer, I. Bey, A. M. Fiori, Q. Li, and R. B. A. Koelemeijer, An improved retrieval of tropospheric nitrogen dioxide from GOME, *J. Geophys. Res.*, *107*(D20), 4437, doi:10.1029/2001JD001027, 2002.
- Martin, R. V., D. J. Jacob, K. Chance, T. P. Kurosu, P. Palmer, and M. Evans, Global inventory of nitrogen oxide emissions constrained by space-based observations of NO_2 columns, *J. Geophys. Res.*, *108*(D17), 4537, doi:10.1029/2003JD003453, 2003.
- Meijer, E. W., P. F. J. van Velthoven, D. W. Brunner, H. Huntreiser, and H. Kelder, Improvement and evaluation of the parametrisation of nitrogen oxide production by lightning, *Phys. Chem. Earth*, *26*, 577–583, 2001.
- van Noije, T. P. C., H. J. Eskes, F. J. Dentener, D. S. Stevenson, K. Ellingsen, M. G. Schultz, O. Wild, M. Amann, C. S. Atherton, D. J. Bergmann, I. Bey, K. F. Boersma, T. Butler, J. Cofala, J. Drevet, A. M. Fiore, M. Gauss, D. A. Hauglustaine, L. W. Horowitz, I. S. A. Isaksen, M. C. Krol, J.-F. Lamarque, M. G. Lawrence, R. V. Martin, V. Montanaro, J.-F. Müller, G. Pitari, M. J. Prather, J. A. Pyle, A. Richter, J. M. Rodriguez, N. H. Savage, S. E. Strahan, K. Sudo, S. Szopa, and M. Van Roozendaal,

- Multi-model ensemble simulations of tropospheric NO₂ compared with GOME retrievals for the year 2000, *Atmos. Chem. Phys. Discuss.*, *6*, 2965–3047, 2006.
- Olivier, J. G. J., and J. J. M. Berdowski, Global emission sources and sinks, in *The Climate System*, edited by J. Berdowski, R. Guicherit, and B. J. Heij, pp. 33–77, Swets & Zeitlinger Publishers, Lisse, 2001.
- Olivier, J. G. J., A. F. Bouwman, K. W. van der Hoek, and J. J. M. Berdowski, Global air emission inventories for anthropogenic sources of NO_x, NH₃ and N₂O in 1990, *Environ. Poll.*, *102*, 135–148, 1998.
- Peters, D. H. M. U., Trend detection and seasonal variation of tropospheric NO₂ over China, Master's thesis, Eindhoven University of Technology, 2005.
- Petricoli, A., P. Bonasoni, G. Giovanelli, F. Ravegnani, I. Kostadinov, D. Bortoli, A. Weiss, D. Schaub, A. Richter, and F. Fortezza, First comparison between ground-based and satellite-borne measurements of tropospheric nitrogen dioxide in the Po basin, *J. Geophys. Res.*, *109*(D15307), doi:10.1029/2004JD004547, 2004.
- Platt, U., Differential optical absorption spectroscopy (DOAS), in *Air Monitoring by Spectroscopic Techniques*, *Chem. Anal.*, vol. 127, edited by M. W. Sigrist, pp. 27–76, Wiley-Interscience, Hoboken N.J., 1994.
- Richter, A., and J. P. Burrows, Tropospheric NO₂ from GOME measurements, *Adv. Space Res.*, *28*, 1673–1683, 2002.
- Richter, A., J. P. Burrows, H. Nüß, C. Granier, and U. Niemeier, Increase in tropospheric nitrogen dioxide over China observed from space, *Nature*, *437*, 129–132, doi: 10.1038/nature04092, 2005.
- Russell, G., and J. Lerner, A new finite-differencing scheme for the tracer transport equation, *J. Appl. Meteorol.*, *20*, 1483–1498, 1981.
- Schaub, D., K. F. Boersma, J. W. Kaiser, A. K. Weiss, D. Folini, H. J. Eskes, and B. Buchmann, Comparison of GOME tropospheric NO₂ columns with NO₂ profiles deduced from ground-based in situ measurements, *Atmos. Chem. Phys. Discuss.*, *6*, 2189–2239, 2006.
- Sillman, S., J. A. Logan, and S. C. Wofsy, The sensitivity of ozone to nitrogen oxides and hydrocarbons in regional ozone episodes, *J. Geophys. Res.*, *95*(D2), 1837–1851, doi: 10.1029/89JD01645, 1990.
- Streets, D. G., and S. T. Waldhoff, Present and future emissions of air pollutants in China: SO₂, NO_x and CO, *Atmos. Environ.*, *34*, 363–374, 2000.
- Streets, D. G., T. C. Bond, G. R. Carmichael, S. D. Fernandes, Q. Fu, D. He, Z. Klimont, S. M. Nelson, N. Y. Tsai, M. Q. Wang, J.-H. Woo, and K. F. Yarber, An inventory of gaseous and primary aerosol emissions in Asia in the year 2000, *J. Geophys. Res.*, *108*(D21), 8809, doi:10.1029/2002JD003093, 2003.

- Tiedtke, M., A comprehensive mass flux scheme for cumulus parameterization in large-scale models, *Mon. Wea. Rev.*, *117*(8), 1779–1800, 1989.
- Wang, X., D. L. Mauzerall, Y. Hu, A. G. R. and E. D. Larson, J.-H. Woo, D. G. Streets, and A. Guenther, A high-resolution emission inventory for Eastern China in 2000 and three scenarios for 2020, *Atmos. Environ.*, *39*, 5917–5933, 2005.
- Wang, Y. X., M. B. McElroy, T. Wang, and P. I. Palmer, Asian emissions of CO and NO_x: Constraints from aircraft and Chinese station data, *J. Geophys. Res.*, *109*(D24304), doi:10.1029/2004JD005250, 2004.
- Yienger, J. J., and H. Levy, Empirical model of global soil-biogenic NO_x emissions, *J. Geophys. Res.*, *100*(D6), 11,447–11,464, doi:10.1029/95JD00370, 1995.

